Dissertation

submitted to the

Combined Faculty of Natural Sciences and Mathematics
of the Ruperto Carola University Heidelberg, Germany

for the degree of

Doctor of Natural Sciences

Presented by

M.Sc. Marcel Kegel

Born in: Speyer, Germany

Oral examination: 15.06.2020

Role of the AMPA receptor auxiliary subunit CKAMP44 in the olfactory bulb

Referees: Prof. Dr. Hannah Monyer

Prof. Dr. Jakob von Engelhardt

Summary

The olfactory bulb is the first processing station of olfactory information. Mitral and tufted cells, which are the output neurons of the olfactory bulb, receive input from olfactory sensory neurons. The activity of the output neurons is controlled by inhibitory periglomerular and granule cells. Periglomerular cells also receive excitatory input from olfactory sensory neurons and provide feedforward inhibition. Little is known about how AMPA receptor number and function in synapses of periglomerular cells is controlled. It is also not well understood how changes in AMPA receptor number of periglomerular cells affect the olfactory bulb network. Here I show with fluorescence *in situ* hybridization that the AMPA receptor auxiliary protein CKAMP44 is expressed at high levels in periglomerular cells, but not or only at low levels in other neurons of the olfactory bulb. With *ex vivo* slice electrophysiology I found that deletion of CKAMP44 decreases AMPA receptor-mediated currents in periglomerular cells. This in turn reduces the inhibition from periglomerular cells onto mitral cells and increases mitral cell activity upon olfactory sensory neuron activation. Data from a computational model of olfactory bulb neuron activity corroborate these findings and indicate that feedforward inhibition from periglomerular cells reduces mitral cell activity in particular during weak or intermediate excitation from olfactory sensory neurons. Behavior experiments showed that the function of the olfactory bulb, at least concerning the differentiation of odors, is not affected by decreased periglomerular cell excitability. Whether other odor functions (e.g. detection threshold) and *in vivo* network activity is affected remains to be investigated.

Zusammenfassung

Der *Bulbus olfactorius* ist die erste Station an der olfaktorische Informationen prozessiert werden. Mitral- und Büschelzellen, die Projektionsneurone des *Bulbus olfactorius*, werden von Riechsinneszellen aktiviert. Die Aktivität der Projektionsneurone wird durch die inhibitorischen Körnerzellen und periglomeruläre Zellen reguliert. Periglomeruläre Zellen werden wie die Projektionsneurone von Riechsinneszellen aktiviert. Dies resultiert in einer sog. *feedforward* Inhibition der Mitralzellen. Wenig ist bekannt zur Regulation der AMPA Rezeptor Anzahl und Funktion in Synapsen der periglomerulären Zellen. Die Auswirkungen einer Änderung der Anzahl von AMPA Rezeptoren von periglomerulären Zellen auf die Aktivität anderer Zellen im *Bulbus olfactorius* ist ebenfalls nur unzureichend untersucht. In meiner Arbeit zeige ich mit Hilfe von Fluoreszenz *In Situ* Hybridisierungen, dass das AMPA Rezeptor auxiliäre Protein CKAMP44 stark in periglomerulären Zellen exprimiert wird, aber nicht oder nur schwach in anderen Zelltypen des *Bulbus olfactorius*. Ich habe durch *ex vivo* Elektrophysiologie in Gehirnschnitten herausgefunden, dass die Deletion von CKAMP44 die durch AMPA Rezeptoren bedingten Ströme in periglomerulären Zellen verringert. Dadurch verringert sich wiederrum die Inhibition der Mitralzellen durch periglomeruläre Zellen und die aus der Aktivierung der Riechsinneszellen resultierende Aktivität der Mitralzellen wird erhöht. Diese Erkenntnisse werden von einem computergestütztem Rechenmodell bestätigt. Weiterhin gibt dieses Rechenmodell Hinweise darauf, dass die *feedforward* Inhibition durch periglomeruläre Zellen die Mitralzellaktivität insbesondere bei schwacher bis mittlerer Aktivität der Riechsinneszellen beeinflusst. Die Funktion des *Bulbus olfactorius*, zumindest in der Unterscheidung von Gerüchen, war in Verhaltensexperimenten nicht beeinflusst durch die reduzierte Erregbarkeit der periglomerulären Zellen. Ob andere Funktionen der Geruchswahrnehmung, z.B. die Schwelle der olfaktorischen Wahrnehmung, und die Netzwerkaktivität *in vivo* beeinflusst werden, bleibt zu ermitteln.

Danksagung

Ich möchte allen danken, die mich in meiner Zeit als Doktorand unterstützt haben. Besonders möchte ich Jakob von Engelhardt für seine großartige Betreuung und Unterstützung danken. Auch möchte ich Hannah Monyer, die sich dazu bereit erklärt hat Erstgutachterin meiner Dissertation zu sein und mir in Lab und TAC Meetings wertvolle Ratschläge gegeben hat, danken. Weiterhin möchte ich auch Christoph Schuster für seinen hilfreichen Beitrag als Mitglied meines TACs danken.

Außerdem möchte ich all meinen Kollegen danken. Eric möchte ich besonders dafür danken, dass er sich viel Zeit genommen hat um mir die Elektrophysiologie beizubringen und mich zu beraten. Hanna möchte ich dafür danken, dass sie mir beim Anpassen des Models geholfen hat, Muhammad für seine Unterstützung bei den FISH Experimenten und Sonia für anregende Diskussionen und die Verbreitung guter Laune. Auch Mona, Michaela, Xufeng, Benedikt, Florian, Anwar, Hristo und Danni möchte ich danken, die mich während der letzten Jahre ebenfalls tatkräftig unterstützt haben und dank denen ich eine schöne Zeit hatte. Auch möchte ich den TAs der von Engelhardt und Monyer Labore danken, ohne die meine Arbeit nicht möglich gewesen wäre insbesondere Barbara, Chiara, Regina und Heike.

Thomas Kuner und Janine Reinert möchte ich für die Bereitstellung des Verhaltenssetups und die Unterstützung bei der Durchführung der Verhaltensversuche danken.

Außerdem bin Kristin dafür dankbar, dass sie mich während meiner Arbeit immer moralisch unterstützt und beraten hat.

Ein besonderer Dank gilt auch meinen Eltern, ohne deren Unterstützung ich es nicht soweit geschafft hätte.

Content

1 Introduction

Living beings perceive their environment via sensory information. Of the four forms of sensory reception, chemoreception is most likely the earliest sensual modality developed by living beings (Wicher 2012). In most animals, olfaction is the predominant form of chemoreception. Olfaction can detect molecules at very low concentrations and can differentiate between a broad range of molecules.

High sensitivity to detect and discriminate odors is of utmost relevance for the survival of many animals. For example, it is important to detect food sources or contaminations at very low concentrations. Odor discrimination plays a role e.g. in the assessment of potential mate's willingness to mate.

Humans, although being primarily visual creatures, are still able to differentiate more than 10000 olfactory stimuli (Menini *et al.* 2004). Even chemically very similar molecules like enantiomeres can be reliably differentiated. Unlike auditory and visual stimuli odorants do not stem from a continuous spectrum, but from a complex, discontinuous distribution, which additionally complicates this task (Imai *et al.* 2010).

1.1 Functional anatomy of the olfactory system

The site of odorant detection are the olfactory sensory neurons. These neurons are located in the olfactory epithelium in the nasal cavity. Odorant molecules enter our nasal cavity during inhalation and are subsequently bound by olfactory sensory neurons, which project to the olfactory bulb. In the olfactory bulb, the information is processed and transmitted to the olfactory cortex.
Olfactory sensory neurons present olfactory receptors on their cilia surface. Each olfactory receptor expresses only one specific olfactory receptor, which bind molecules with specific molecular features (Menini *et al.* 2004). Mammals have approximately 400 to 1000 genes that encode olfactory receptors (Gaillard *et al.* 2004, Niimura & Nei 2007). This underlines the importance of having an olfactory system with the ability to detect a wide range of olfactory receptors for mammals. In this thesis, I will focus on the mouse olfactory bulb for experimental reasons.

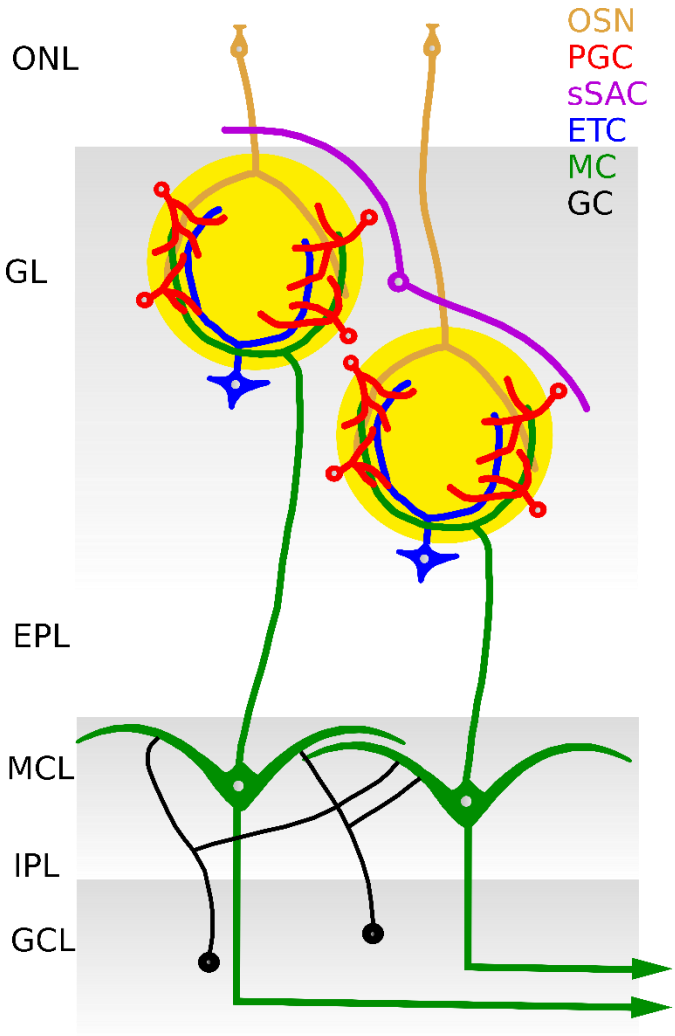

Figure 1: Schematic representation of the layer structure of the olfactory bulb and selected cell types. Abbreviations of layers is given on the left and cell types legend is color coded in the top right corner. ONL: olfactory nerve layer, GL: glomerular layer, EPL: external plexiform layer, MCL: mitral cell layer, IPL: internal plexiform layer, GCL: granule cell layer, OSN: olfactory sensory neuron, PGC: periglomerular cell, sSAC: superficial short-axon cell, ETC: external tufted cell, MC: mitral cell, GC: granule cell (generated according to data from Nagayama et al. 2014)

1.2 Olfactory bulb

Olfactory sensory neurons' axons project to the olfactory bulb. Information received from olfactory sensory neurons is processed by a complex neuronal network and subsequently send to the olfactory cortex. The neuronal network of the olfactory bulb is divided into 6 anatomically distinct layers. Figure 1 shows a simplified scheme of the layered cellular organization. The layers listed by increasing distance to the

surface are: olfactory nerve layer, glomerular layer, external plexiform layer, mitral cell layer, internal plexiform layer and granule cell layer (Scott *et al.* 1993). The olfactory nerve layer contains the axons of the olfactory sensory neurons, which project to the glomerular layer. The term *glomerular layer* originates from the structurally distinct, spherical formations, the so-called glomeruli. These glomeruli are areas in which the axons of the olfactory sensory neurons form synapses with the dendrites of periglomerular, mitral and tufted cells. The fact that glomeruli do not contain cell bodies leads to the structural difference to the surrounding region (Nagayama *et al.* 2014, Scott *et al.* 1993).

Besides the glomeruli themselves, the glomerular layer contains periglomerular, superficial short-axon and external tufted cells. The next deeper layer is the external plexiform layer. Neurons are sparsely distributed in the external plexiform layer, which explains its plexiform appearance. The external plexiform layer contains tufted cells and different types of interneurons. The level following the external plexiform layer is the mitral cell layer. The mitral cell layer is a thin layer of densely packed mitral and smaller granule cells. The innermost layer is the granule cell layer. It is separated from the mitral cell layer by the thin internal plexiform layer, which contains no cell bodies. The eponymous granule cells and deep short axon cells are located in the densely packed granule cell layer (Nagayama *et al.* 2014, Scott *et al.* 1993).

The organization of the integration of olfactory input in single glomeruli is of functional relevance, as all olfactory sensory neurons that project to one glomerulus express the same olfactory receptor. In turn several glomeruli can be innervated by sensory neurons expressing the same receptor (Treloar *et al.* 2002). This specific organization causes that the same odor or the same odor mixture always activates the same pattern of glomeruli. The task of the olfactory bulb is to decorrelate and relay to higher brain regions information contained in these glomerular activation patterns (Mori *et al.* 2006).

1.3 Functional role of interneurons in the olfactory bulb

One of the prominent general functions of interneurons in neuronal networks is the control of neuronal activity in these networks (Kee *et al.* 2015, Allen & Monyer 2015). In the olfactory bulb, the most abundant interneurons are periglomerular and granule cells (Parrish-Aungst *et al.* 2007). Both cell types are replenished by newborn neurons throughout the animal's life. In the olfactory system, neurogenesis occurs in the subventricular zone. From there, newborn cells migrate along the rostral migratory stream to the olfactory bulb, where they integrate into the existing neuronal network (Lledo *et al.* 2006).

Periglomerular cells inhibit mitral and external tufted cells. The class of periglomerular cells is heterogeneous. One possibility to categorize them is via their connectivity. Periglomerular cells of type-I synapse with olfactory sensory axons and periglomerular cells of type-II do not receive direct input from olfactory sensory neurons (Kosaka *&* Kosaka 2004). Similarly, periglomerular cells can be categorized according to their primary source of input into olfactory nerve driven or external tufted cell driven cells (Kiyokage *et al.* 2010). Type-II periglomerular cells have to be mainly driven by external tufted cells. Type-I periglomerular cells could belong to both categories, since they could receive their dominant input either from olfactory sensory neurons or external tufted cells.

Another possibility is to classify periglomerular cells according to their neurotransmitters. Most periglomerular cells are GABAergic with a smaller dopaminergic subpopulation. Specific molecular markers can also be used for classification. Three sub-groups of significant size are calretinin (CR), calbindin (CB) and tyrosine hydroxylase (TH) expressing cells (figure 2). Expression of these three marker proteins shows little overlap (Kosaka & Kosaka 2007).

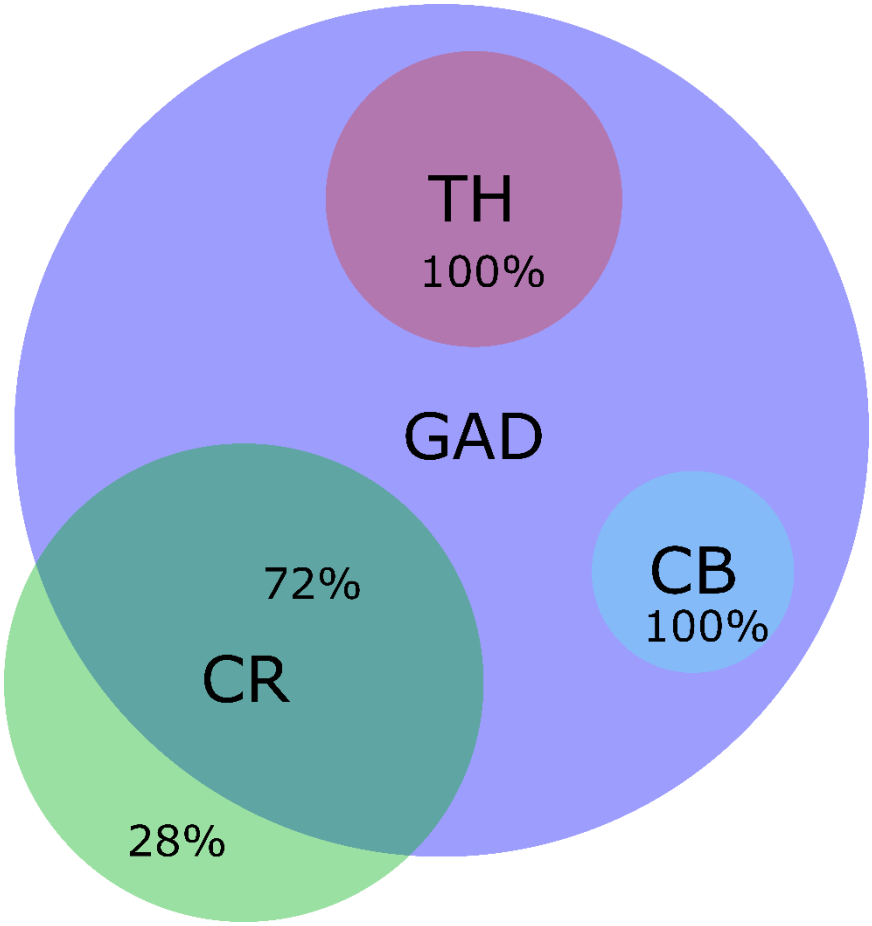

Figure 2: Molecular marker expression in periglomerular cells (generated according to data from Kosaka & Kosaka 2007)

1.4 Intra- and interglomerular circuits in the olfactory bulb

Periglomerular and granule cells are a fundamental part of a complex network to process olfactory information received from olfactory sensory neurons (figure 3). Both intra- and interglomerular circuits process information in the olfactory bulb.

In the following paragraph, four functional components of olfactory bulb circuits will be described in more detail (see also figure 4 to 7 in which only those components are shown):

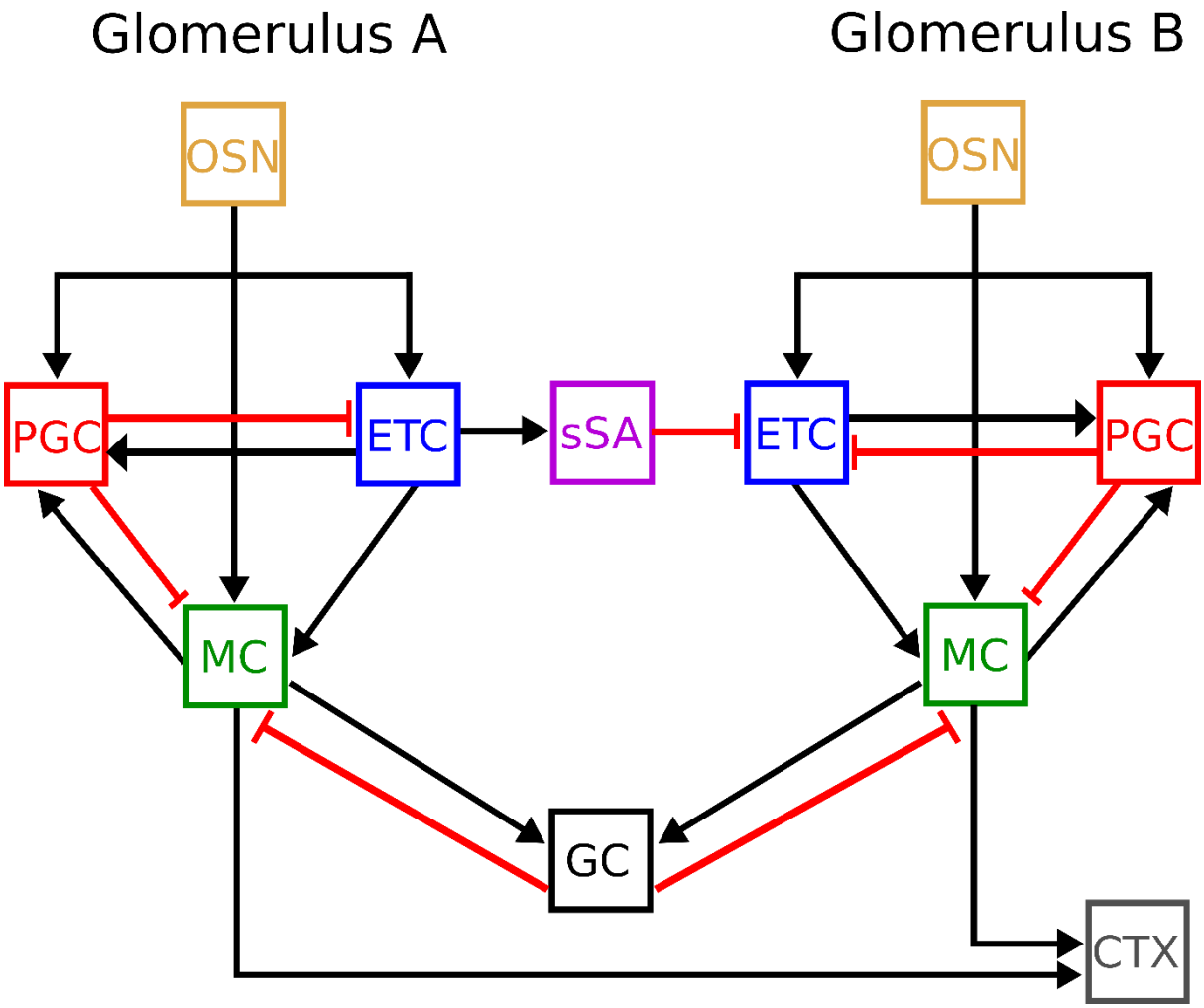

Figure 3: Schematic representation of the olfactory bulb network. Black lines indicate excitatory connections, red lines inhibitory connections. Abbreviations: OSN: olfactory sensory neurons, PGC: periglomerular cell, ETC: external tufted cell, sSA: superficial short-axon cell, MC: mitral cell, GC: granule cell, CTX: cortex (generated according to data from Nagayama et al. 2014)

1. Intraglomerular feedforward and feedback inhibition between periglomerular und mitral cells

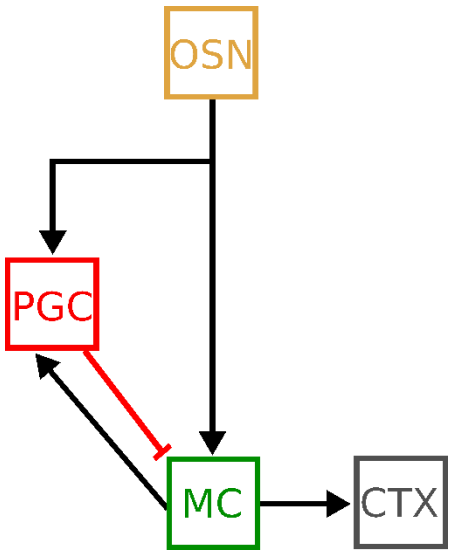

Figure 4: Schematic representation of an intraglomerular circuit, consisting of periglomerular and mitral cells. Abbreviations: OSN: olfactory sensory neuron, PGC: periglomerular cell, MC: mitral cell, CTX: cortex

Dendrites of single mitral and periglomerular cells are exclusively located in one glomerulus (Price & Powell 1970, Mori *et al.* 1983, Pinching & Powell 1971). Olfactory sensory neurons form synapses with both mitral cells and type-I periglomerular cells. Mitral and periglomerular cells are connected by reciprocal dendrodendritic synapses. Periglomerular cells inhibit mitral cells, while mitral cells excite periglomerular cells (Murphy *et al.* 2005). This constellation forms both a feedforward inhibition as well as feedback inhibition (figure 4). One hypothesized function of this feedforward inhibition is to prevent mitral cell activation of weakly activated glomeruli. The input resistance of periglomerular cells is lower than that of mitral cells, therefore periglomerular cells reach their maximum activity at lower olfactory neuron input strength than mitral cells (Chen *et al.* 2002, Shen *et al.* 1999). Consequently, only mitral cells of glomeruli that receive strong input are active. Similar odors cause overlapping glomerular ensemble activation. This ensemble overlap is reduced if mitral cells of weakly activated glomeruli are silenced by feedforward inhibition of periglomerular cells (Cleland & Sethupathy 2006).

2. Intraglomerular synchronization between mitral cells

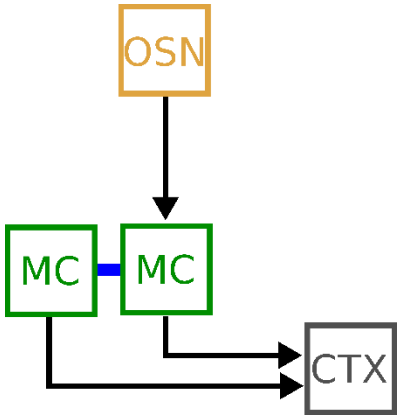

Figure 5: Schematic representation of an intraglomerular circuit, consisting of mitral cells. Black lines indicate excitatory connections, red lines inhibitory connections, blue lines indicate electric coupling via gap-junctions. Abbreviations: OSN: olfactory sensory neuron, PGC: periglomerular cell, MC: mitral cell, CTX: cortex

Mitral cells projecting dendrites to the same glomerulus show synchronized activity. This synchronicity stems from synchronized inputs, but also from electrical coupling between mitral cells mediated by gap-junctions (Schoppa & Westbrook 2001, Christie *et al.* 2005, see figure 5).

3. Interglomerular inhibition via external tufted and superficial short-axon cells

The first interglomerular circuit is established by external tufted cells which are innervated by olfactory sensory neurons and form an excitatory network with long-range GABAergic superficial short-axon cells that inhibit external tufted cells in other glomeruli. Since external tufted cells excite mitral cells, this part of the circuit conveys interglomerular inhibition. Interglomerular inhibition may normalize mitral cell activity for odor concentrations. Thereby, the overall mitral cell activity is kept stable at different odor concentrations (De Saint Jan *et al.* 2009, Kiyokage *et al.* 2010, Whitesell *et al.* 2013, Nagayama *et al.* 2014, Linster & Cleland 2009, see figure 6).

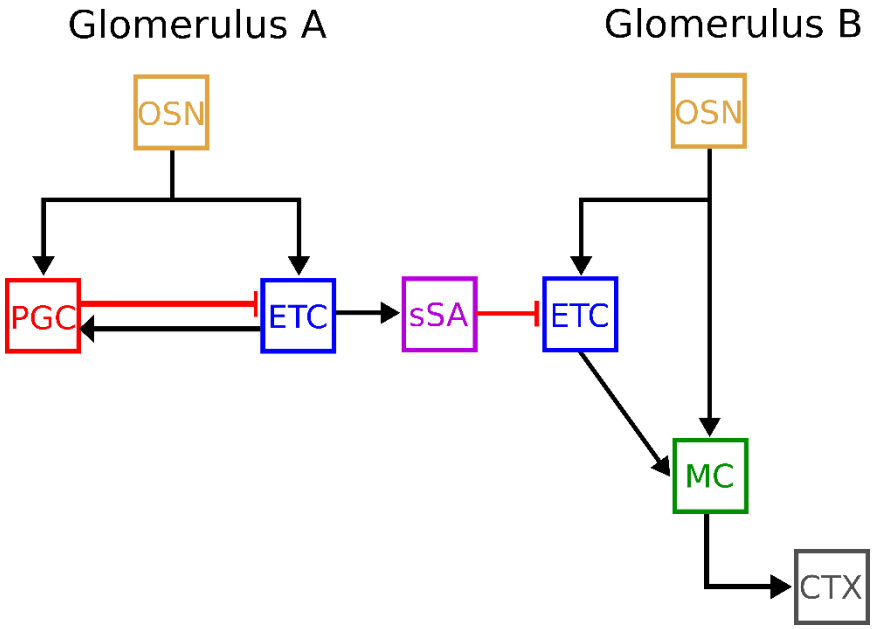

Figure 6: Schematic representation of an interglomerular circuit I. Black lines indicate excitatory connections, red lines inhibitory connections. Abbreviations: OSN: olfactory sensory neuron, PGC: periglomerular cell, ETC: external tufted cell, sSA: superficial short-axon cell, MC: mitral cell, CTX: cortex

4. Interglomerular inhibition conveyed by granule cells

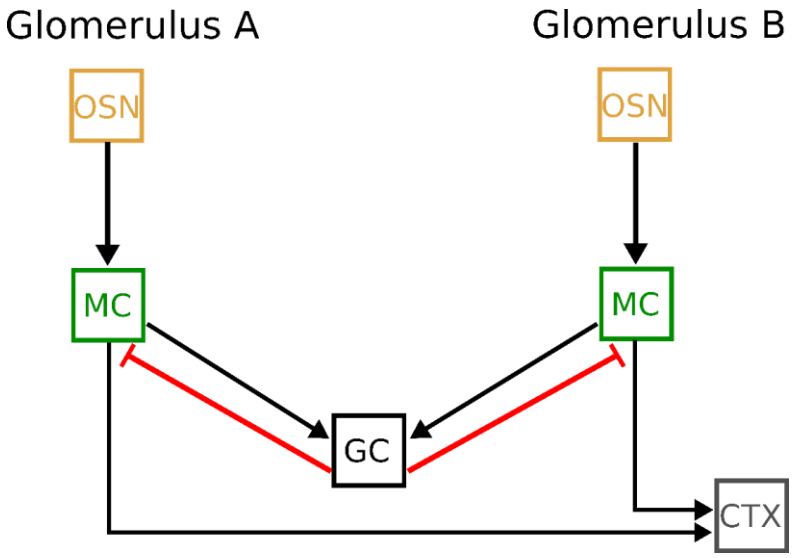

Figure 7: Schematic representation of an interglomerular circuit II. Black lines indicate excitatory connections, red lines inhibitory connections. Abbreviations: OSN: olfactory sensory neurons, MC: mitral cell, GC: granule cell, CTX: cortex

The other circuit of interglomerular inhibition described here is formed by mitral and granule cells. Granule cells form, like periglomerular cells, reciprocal dendrodentritc synapses with mitral cells. Unlike periglomerular cells, granule cells do not form synapses only with mitral cells belonging to the same glomerulus, but innervate several mitral cells from different glomeruli and thereby generate an interglomerular inhibitory network (Urban & Sakmann 2002, see figure 7). This interglomerular connection is hypothesized to enhance contrast between strongly and weakly activated mitral cells (Mori *et al.* 1999).

1.5 AMPA receptors

AMPA receptors are the most abundant receptors in the central nervous system. Due to their characteristic gating behavior, AMPA receptors conduct the fast component of excitatory synaptic currents. AMPA receptors are cation-channels that are permeable for sodium, potassium and in some cases calcium ions. This ion permeability leads to a reversal potential of native AMPA receptors of around 0-10 mV, depending on the ionic composition of the extra- and intracellular milieu.

AMPA receptors are tetramers, built out of different combinations of the four distinct subunits, GluA1, GluA2, GluA3 and GluA4. Most AMPA receptors in the brain are heterotetramers, but homomers are functional as well. This increases the number of possible structurally and functionally different AMPA receptors (Swanson *et al.* 1997). The typical structure of an AMPA receptor is shown in figure 8. Each of the single AMPA receptor subunits has a ligand binding site and three transmembrane domains. The pore is formed by another domain within, but not passing through, the plasma membrane, when the tetramer is assembled. Consequently, the final receptor at the cell surface contains four binding sites for glutamate (one for each subunit). After binding of agonists to two or more binding sites, the pore opens. If more binding sites are occupied by agonists, the current increases. The current is therefore dependent on agonist concentration (Rosenmund *et al.* 1998).

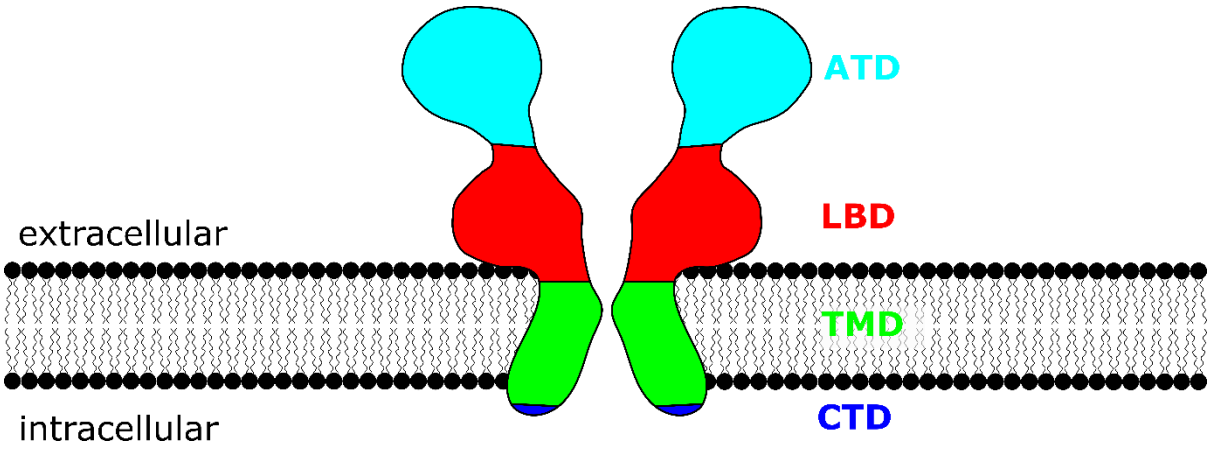

Figure 8: Schematic architecture of an AMPA receptor. Abbreviations: ATD: amino-terminal domain. LBD: ligand binding domain, TMD: transmembrane domain, CTD: C-terminal domain.

Many properties of AMPA receptors depend on their subunit composition. Especially the presence of the GluA2 subunit drastically alters electrical properties of the receptors. Hence, AMPA receptors that contain GluA2 are impermeable to calcium, show a lower conductance and a specific voltage dependency at positive potentials. These electrical characteristics of GluA2 containing receptors mainly arise from one amino acid in the pore-building region, where one codon of the pre-mRNA is modified to encode for an arginine instead a glutamine (Källman *et al.* 2003, Wright & Vissel 2012, Pachernegg *et al.* 2015).

Other modifications that increases AMPA receptor heterogeneity are alternative splicing and post-translational modifications, like phosphorylation (Sommer *et al.*1990, Monyer *et al.* 1991, Wang *et al.* 2005).

In the olfactory bulb AMPA receptor subunits are expressed differentially in different layers. Considering the mitral cell, granule cell and glomerular layers, all layers show expression of all subunits, but at different intensities. GluA1 is most strongly expressed in the glomerular layer. GluA2 and GluA 4 are expressed in all layers similarly. GluA 3 is most strongly expressed in the mitral and granule cell layer (Montague & Greer 1999, Lein *et al.* 2007).

1.6 AMPA receptor-interacting proteins

As described in the last paragraph, the specific subunit composition is relevant for properties of AMPA receptor-mediated currents. However, research from the past twenty years showed that the presence of AMPA receptor-interacting proteins has a strong effect on AMPA receptor function. AMPA receptor interacting proteins can influence subcellular location and gating properties of AMPA receptors (von Engelhardt *et al.* 2010, Khodosevich *et al.* 2014, Schwenk *et al.* 2009, Tomita *et al.* 2003). Today, approximately 30 AMPA receptor interacting proteins are known. A sub-group of AMPA receptor-interacting proteins are AMPA receptor auxiliary subunits. These proteins influence not only AMPA receptor trafficking, but also gating and localization on the cell surface. There are different families of AMPA receptor auxiliary subunits, namely transmembrane *AMPA* receptor regulatory proteins (TARPs), Cornichons (CNIH), Germ Cell-Specific Gene 1-Like Protein (GSG1L) and *Cystine-knot* AMPA receptor-modulating proteins (CKAMPs, also known as Shisa family) (Schwenk *et al.* 2009, Schwenk *et al.* 2012, Farrow *et al.* 2015, von Engelhardt 2019).

The TARP family consists of TARP-γ2, TARP-γ3, TARP-γ4, TARP-γ5, TARP-γ7 and TARP-γ8. Based on sequence and functional similarities, the family can be further subdivided into type-1 (TARP-γ2, TARP-γ3, TARP-γ4, TARP-γ8) and type-2 (TARP-γ5 and TARP-γ8) (Jackson & Nicoll 2011). The TARP family is the biggest with six members. The second largest family is the CKAMP family, consisting of four members, CKAMP39, CKAMP44, CKAMP52 and CKAMP59. The numbers correspond to their molecular weight in kDa. The Cornichon family consists of CNIH2 and CNIH3. No family members of GSG1L are known (von Engelhardt *et al.* 2010, Farrow *et al.* 2015, Schwenk *et al.* 2009, Boudkkazi *et al.* 2014, Schwenk *et al.* 2012).

Auxiliary subunits differentially modulate AMPA receptor function. The function of a specific AMPA receptor auxiliary subunit further depends on the subunit composition of the AMPA receptor (Kessels *et al.* 2009). Additionally, the presence of other AMPA receptor auxiliary subunits in the AMPA receptor complex influences auxiliary subunit function (Kato *et al.* 2010). Considering that expression of AMPA receptor interacting proteins is region and cell type specific, AMPA receptor function is modified differently in different cell types (Jacobi & von Engelhardt 2017). While the function of certain AMPA receptor interacting proteins in specific cell types has been investigated, the

overall benefit of this complex regulatory machinery and its impact on network activity remains unknown.

1.7 CKAMP44

In my thesis, I investigated the function of the auxiliary subunit CKAMP44. The structure of CKAMP44 is shown in figure 9. The extracellular domain contains the N-terminal region and a cysteine rich region which forms the eponymous cysteine-knot. CKAMP44 has one transmembrane domain and an intracellular PDZ domain interacting motif (von Engelhardt *et al.* 2010). CKAMP44 is expressed highly in dentate gyrus granule cells and lateral geniculate nucleus (LGN) relay neurons. CKAMP44 influences trafficking, localization and function of AMPA receptors. Hence, deletion of CKAMP44 reduces the number of synaptic AMPA receptors (Khodosevich *et al.* 2014, Chen *et al.* 2018).

Recovery from desensitization of AMPA receptors is faster in CKAMP44$^{-/-}$ mice. This explains an increase in the paired-pulse ratio of synaptic currents in dentate gyrus granule cells and LGN relay neurons of CKAMP44$^{-/-}$ mice. *In vivo* recording LGN relay neurons showed a higher action potential frequency in CKAMP44$^{-/-}$ mice due to these changes in short-term plasticity (Khodosevich *et al.* 2014, Chen *et al.* 2018). Not all synapses are affected equally by CKAMP44 deletion, even if they contain the same amount of CKAMP44. Relay neurons form retinogeniculate and corticogeniculate synapses. At the retinogeniculate synapse CKAMP44 affects short-term plasticity, but not at the corticogeniculate synapse. For CKAMP44 to affect short-term plasticity, short-term plasticity has to be affected by AMPA receptor desensitization. The retinogeniculate synapse of relay cells in the LGN has a high release probability and glutamate spillover takes place. Therefore, short-term plasticity is affected by AMPA receptor desensitization. At corticogeniculate synapses the release probability is low. Therefore, AMPA receptor desensitization does not affect short-term plasticity (Chen *et al.* 2018, Granseth *et al.* 2002).

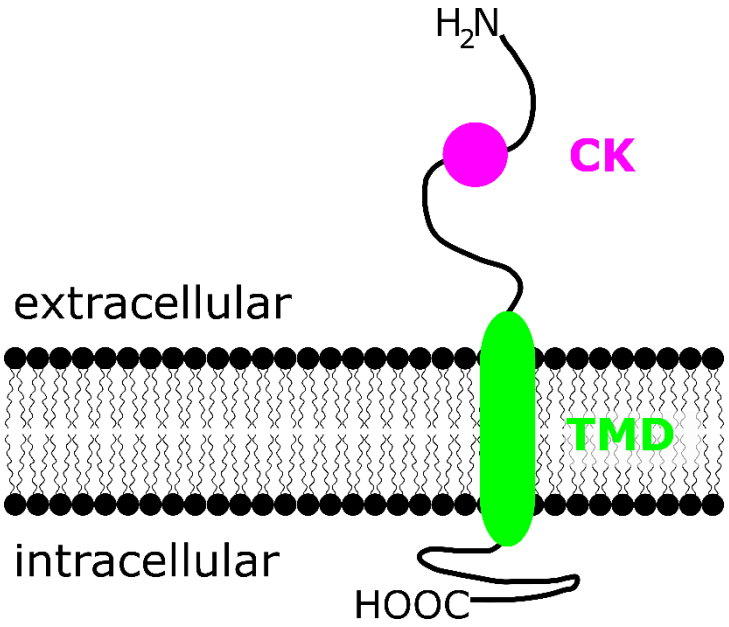

Figure 9: Schematic architecture of CKAMP44. Abbreviations: CK: cysteine-knot, TMD: transmembrane domain (generated according to data from von Engelhardt et al. 2010).

1.8 Aim of study

The aim of this study is to analyze the function of CKAMP44 in the olfactory bulb of mice. CKAMP44 expression is particularly high in the periglomerular layer, but low or absent in the granule cell and mitral cell layer as evidenced by *in situ* hybridization experiments (von Engelhardt *et al.* 2010, see figure 10). Since the most common cells in the periglomerular layer are periglomerular cells, I additionally want to use CKAMP44 as a tool to analyze the function of periglomerular cells in the olfactory bulb network. This would also further our understanding of the olfactory bulb network.

The specific questions of the thesis are:

1) Which olfactory bulb cell types express CKAMP44?

   This question was addressed by double fluorescent *in situ* hybridization experiments.

2) In which cell types are AMPA receptor-mediated currents affected by CKAMP44 deletion?

   Electrophysiological measurements of spontaneous and evoked currents were employed to answer this question.

3) Is short-term plasticity affected by CKAMP44 deletion in cell types with strong CKAMP44 expression?

   Electrophysiological measurements of paired evoked currents were employed to address this question.

4) Is network activity modulated by CKAMP44 deletion?

   This question was approached by electrophysiological recordings in cells not directly affected by the CKAMP44 deletion.

5) Is olfactory bulb function affected by CKAMP44 deletion?

   Behavioral odor discrimination experiments were employed to address this question.

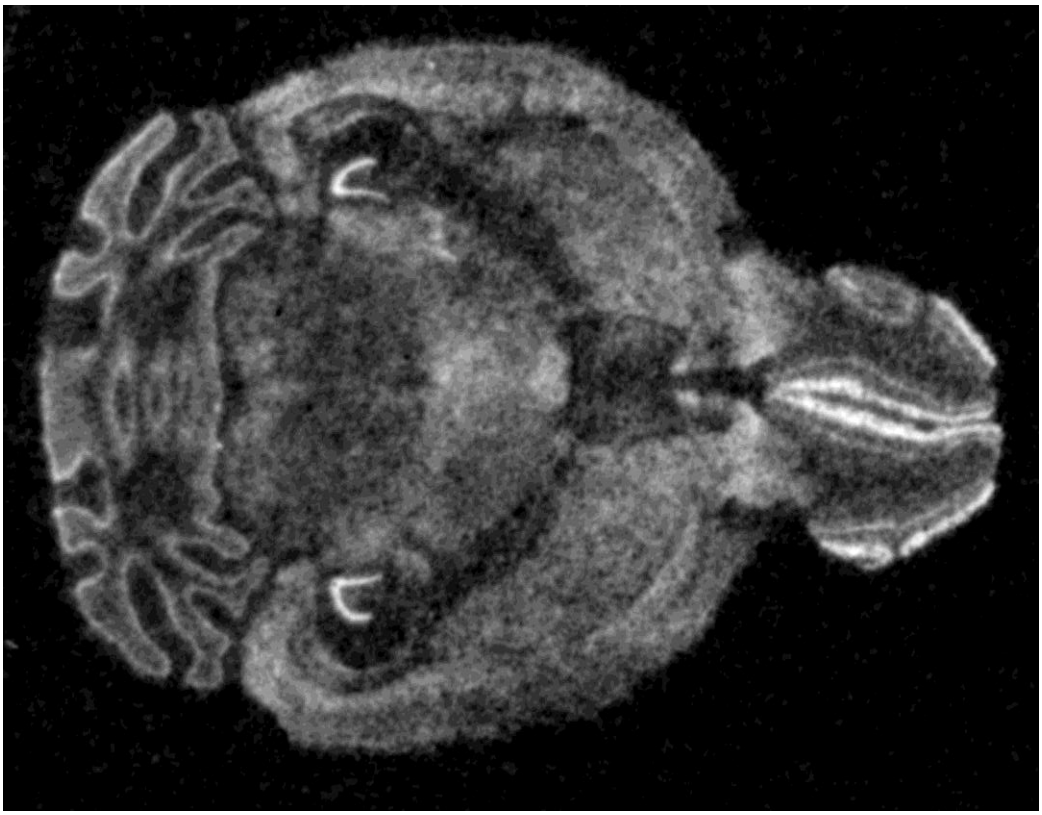

Figure 10: In situ hybridization showing the expression of CKAMP44 in the adult mouse brain (von Engelhardt et al. 2010).

2 Methods

2.1 Mice

All animals were bred and housed under specific-pathogen-free conditions. Mice had *ad libitum* access to both water and food. Up to three animals were housed in type II filtertop cages in the animal holding facility of the German Cancer Research Center in Heidelberg or the Translational Animal Research Center in Mainz. All animal experimentation was carried out in accordance with local animal welfare regulations. All mice belonged to the C57BL/6N substrain. CKAMP44 deficient mice were generated as described previously (von Engelhardt *et al.* 2010).

2.2 Fluorescent *in situ* hybridization

Fluorescent *in situ* hybridization (FISH) experiments were performed with the ViewRNA™ ISH Cell Assay Kit and ViewRNA™ Probe Sets. Double FISH stainings were performed always including the shisa9 probe and calbindin1, calbindin2 or glutamate decarboxylase 1 probe, respectively. The protein names of the genes will be used in my thesis for ease of understanding even if the genes are discussed (*Shisa9*: CKAMP44, C*albindin1*: CB, *Calbindin2*: CR, *Gad1*: glutamate dehydrogenase 67 (GAD67)). Brains were removed while keeping the olfactory bulb intact. After removal, brains were shortly washed in diethyl pyrocarbonate (DEPC)-treated phosphate-buffered saline (PBS). Tissue paper was used to remove excessive PBS and brains were placed on tin foil located on a metal plate on dry ice. Upon complete freezing the brain was wrapped in tin foil and stored at -80 °C until cutting. 12 µm thick horizontal slices on Superfrost™ Plus Slides (Thermo Fischer Scientific, USA) were prepared with a cryotome. Slices were fixed in Roti®-Histofix 4 % (Carl Roth, Deutschland) for 14 to 18 h. Subsequently, slices were washed in DEPC-treated PBS, dehydrated by submersion for 2 min in each ethanol solution of increasing concentration (50, 70, 100%). To complete dehydration slices were incubated at 60 °C for 1 h. At this point it was possible to store slice for several weeks and -80 °C in a sealed box. For rehydration slices were submerged for 2 min in each ethanol solution of decreasing concentration (100%, 70%, 50%). To finish hydration, slices were

washed with DEPC-treated dH_2O twice for 1 min and dipped in DEPC-treated PBS. After removing as much excess solution as possible from the slide, while ensuring that the slices do not dry completely (this procedure will be referred to as “removal of excess solution”), prewarmed protease solution (ViewRNA™ ISH Cell Assay Kit) was pipetted on the slices and the solution was covered with parafilm to prevent loss of solution and adequate distribution. The slices were incubated at 40°C for 10 min for permeabilization. Slices were then dipped twice in DEPC-treated PBS and incubated for 3 min in Roti®-Histofix 4 %, followed by a two times repeated washing step with DEPC-treated PBS and gentle shaking. Excess solution was removed and a working probe mix (ViewRNA™ ISH Cell Assay Kit) distributed on the slices and covered with parafilm. Overnight incubation at 40°C in a humidity chamber allowed for binding of the probes to their target mRNA sequences. Slices were then washed with wash buffer C (ViewRNA™ ISH Cell Assay Kit) 3 times for 2 min each while being shaken vigorously. After removal of excess solution slices were covered with the preamplifier mix (ViewRNA™ ISH Cell Assay Kit), which contains DNA fragments able to bind the probes. The preamplifier mix was covered with parafilm and incubated at 40 °C for 1 h. This was followed by washing the slices with wash buffer C (ViewRNA™ ISH Cell Assay Kit) 3 times for 2 min each while shaking them vigorously. Excess solution was removed and the amplifier mix (ViewRNA™ ISH Cell Assay Kit) distributed on the slices for 1 h of incubation at 40 °C. The amplifier mix contains DNA binding to sequences of the preamplifier mix, which enlarges the DNA structure which can be labeled (see figure 11). A washing step with wash buffer C and vigorous shaking for 2 min was repeated 3 times. All following steps were performed while protecting the slices from light to prevent bleaching. The label probe mix (ViewRNA™ ISH Cell Assay Kit) was distributed on the slices and incubated for 1 h at 40°C. The fluorescent label probes bind specifically to the amplifier DNA fragments, which leads to further signal amplification. The slices were washed in wash buffer C four times while shaking them vigorously for 3-10 min per repetition. In a further washing step, slices were submerged in DEPC-treated PBS twice for one minute. After removal of excess solution, slices were covered with DAPI working dilution (ViewRNA™ ISH Cell Assay Kit) and incubated at room temperature for 10 min. For washing, slices were submerged twice in DEPC-treated PBS and once in DEPC-treated dH_2O for 1 min. Excess solution was removed and the slices were left to dry for approximately 10 minutes. Slices were mounted with Prolong Gold Antifade (Thermo Fisher Scientific,

USA). And left to dry over-night. Afterwards slices could be stored for over one month at 4 °C in a sealed box. Imaging was performed with a Leica SP5 confocal microscope using the Leica Application Suite Advanced Fluorescence software. To quantify the mRNA-staining single dots were counted after contrast enhancement in ImageJ.

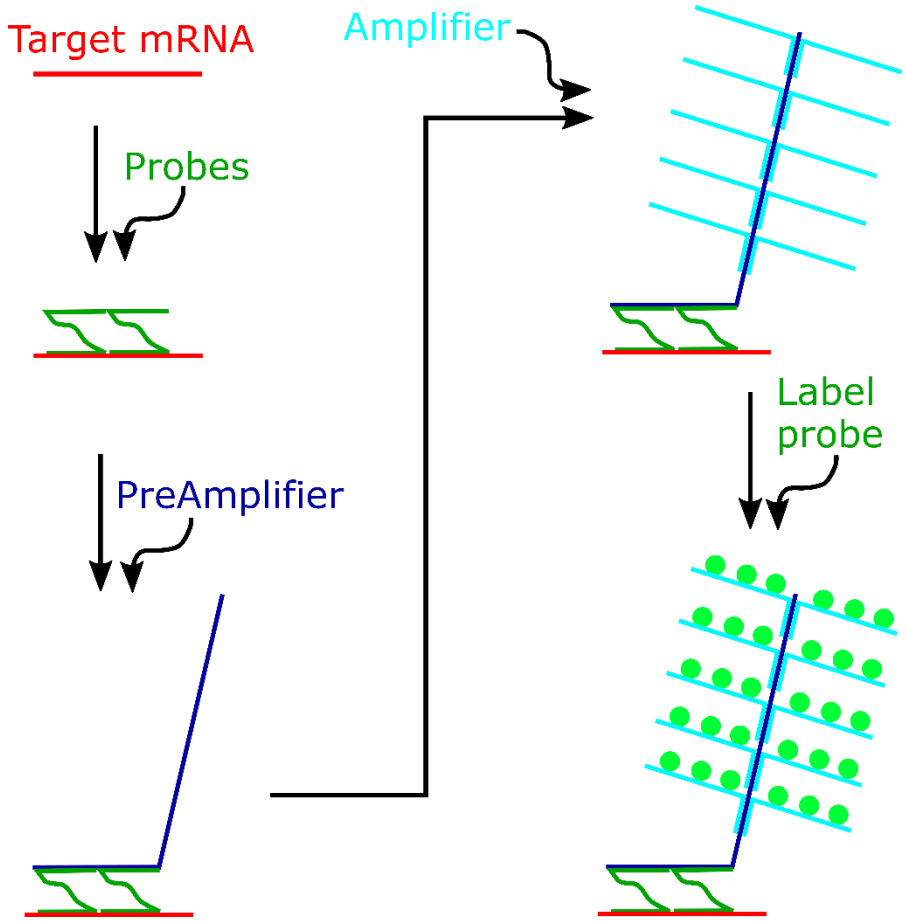

Figure 11: Schematic representation of FISH labelling method.

2.3 Electrophysiology

2.3.1 Cholin-based cutting solution and artificial cerebrospinal fluid

The cutting solution (in mM: 87 NaCl, 25 $NaHCO_3$, 37.5 choline chloride, 2.5 KCl, 1.25 NaH_2PO_4, 0.5 $CaCl_2$, 7 $MgCl_2$, 25 glucose) contained additional choline and less sodium in comparison to the artificial cerebrospinal fluid (ACSF) (in mM: 125 NaCl, 25 $NaHCO_3$, 2.5 KCl, 1.25 NaH_2PO_4, 2 $CaCl_2$, 1 $MgCl_2$, 25 glucose) to decrease harmful neuronal

activity during slice preparation. Both solutions were continuously oxygenated with carbogen (95% O_2 and 5% CO_2) to adjust the oxygen concentration and the pH value to 7.4. 1x solutions were diluted from 10x stock solutions without $CaCl_2$, $MgCl_2$ and glucose. These components were added shortly before usage. The 10x ACSF was stored at room temperature (RT). The 10x cutting solution and the 1x solutions were stored at 4°C.

2.3.2 Acute brain slices

Mice were anesthetized with isoflurane. Adequate depth of anesthesia was confirmed by pedal and tail-pinch reflexes. Mice were then decapitated and the skull bone covering the brain removed and the brain transferred to 4°C cutting solution. The olfactory bulb was cut into 300 µm coronal slices with a Leica VT1200 S vibratome. The slices were transferred to 37°C cutting solution. After 20 min incubation they were transferred to 37°C ACSF for another 20min, after which they were transferred to RT ACSF. Slices were kept at least 20 min at RT before electrophysiological recordings were performed.

2.3.3 Setup

The setup is built up as follows: A custom made slice chamber contains the slice which is held in place by a grid (a thin U-formed platin rod to which single filaments of floss are clued). The slice chamber is continuously perfused with ACSF at a flow rate of 1ml/min. The perfusion system is driven by a peristaltic pump (120S, Watson Marlow, United Kingdom). A microscope (SliceScope, Scientifica, United Kingdom) with a 4x and a 40x objective (PLCN4x-1-7 / LUMPLFLN40xW, Olympus, Japan) was used for magnification. Infra-red light was provided by a LED lamp (SS-3200-10, Scientifica, United Kingdom). Infra-red light enables imaging deeper in the slice. To enhance contrast a differential interference contrast system was used (Olympus, Japan). Microscope movement was controlled with a keypad (Patchpad P pad lite, Scientifica UK) via a remote controller (1U rack, Scientifica, United Kingdom). For fluorescence excitation/detection a mercury lamp (USH-1020L, Olympus, Japan) fixed in a light

housing (U-LH100HG-1-7, Olympus, Japan) powered by the power supply U-RFL-T (Olympus, Japan) was employed. The light housing was connected to the microscope via a BX-URA2-5 adapter which contained the filter cubes U-MNG2 and U-N49002 (Olympus, Japan). Slices were imaged with a XM10 CCD camera (Olympus, Japan) and the cellSense Entry software (Olympus, Japan).

Cells were electrophysiological recorded via a chlorinated silver electrode inserted into a borosilicate glass pipette, which was filled with intracellular solution and connected to a probe. The probe was connected to an EPC10 USB amplifier (HEKA, Germany). Signals from the amplifier were decoded and recorded by the PatchMaster software (HEKA, Germany). Protocols for electrophysiological recordings were sent to the amplifier by the PatchMaster software. Axons were electrically stimulated with a chlorinated silver electrode inserted into a borosilicate glass pipette with an opening of 4-8 µm and filled with extracellular solution. The stimulation electrode was connected to a stimulus isolator (A365, WPI, USA). The stimulus isolator was controlled by the PatchMaster software via the amplifier. Two chlorinated silver bath electrodes were used, one for the recording and one connected to the stimulus isolator. Both the probe and the stimulation electrode holder were mounted on micromanipulators (Mini 25-ZR, Luigs & Neumann, Germany) controlled by a keypad (SM-7, Luigs & Neumann, Germany) via a remote controller (SM-7, Luigs & Neumann, Germany).

It was necessary to be able to apply pressure to the pipette for patching. To achieve this a tube system was installed with a pressure gauge, syringes and a three-way valve.

The microscope and the micromanipulators were located on an optical table (Vision IsoStation, Newport, USA) and enclosed by a custom-build faraday cage to reduce noise.

Patch pipettes were pulled from borosilicate-glass capillaries (Hilgenberg, Germany) with a micropipette puller (P-1000, Sutter Instrument, USA).

2.3.4 Whole cell recordings

Healthy cells were identified with the 40x objective. The patch pipette was lowered into the extracellular solution and positive pressure between 20 and 60 mbar depending

on cell type was applied. To monitor the size of the pipette tip opening and potential blockages, a voltage step of 5 mV (duration: 500 µs) was repeatedly applied and the pipette resistance and resulting current visually monitored with PatchMaster. Cells were approached with the pipette until an indentation on the cell surface due to the positive pressure was visible. Then instead of positive pressure, negative pressure was applied and the control voltage was set to -70 mV in PatchMaster. Upon the seal resistance exceeding 1 GΩ the pressure was released. A seal was considered adequate for leak currents lower than 10 pA. Cells were opened by applying simultaneously a short pressure pulse and a short voltage pulse (800 mV for 0.05 ms). After opening, cell access was monitored by measuring the amplitude of the initial current caused by the 5 mV voltage step. All data was recorded with PatchMaster. Liquid junction potential was not corrected for. All recordings were performed at RT.

2.3.5 Identification of cell types

Cells were identified by layer (figure 1), soma size according to Nagayama *et al.* 2014 and in the glomerular layer by morphology according to the original classification by Pinching & Powell 1971. To assess morphology, cells were filled with lucifer yellow during recording and imaged using the setup's fluorescence detection.

2.3.6 Miniature excitatory postsynaptic currents

Miniature excitatory postsynaptic currents (mEPSC) were recorded at -70 mV holding potential and tetrodotoxin (TTX, 1 µM), gabazine (10 µM) and 2-Amino-5-phosphonovaleriansäure (APV, 50 µM) were added to the ACSF. The intracellular solution contained (in mM): 130 potassium gluconate, 10 Hepes, 10 phosphocreatine disodium salt hydrate, 10 sodium D-gluconate, 4 ATP magnesium salt, 4 NaCl, 0.3 GTP sodium salt hydrate, 1mM lucifer yellow CH, pH was adjusted with KOH to 7.2. Cell access was monitored by applying a 5 mV voltage step every 10 s. Data was analyzed semi-automatically using pClamp 10.4 software after converting Patchmaster Files to Igor files.

2.3.7 AMPAR/NMDAR ratio

Gabazine (10 µM) was added to the extracellular ACSF. The intracellular solution contained (in mM): 120 caesium gluconate, 10 CsCl, 10 Hepes, 10 phosphocreatine disodium salt hydrate**,** 8 NaCl, 2 ATP magnesium salt, 0.3 GTP sodium salt hydrate, 0.2 EGTA, pH was adjusted with CsOH to 7.3**.** First, AMPA receptor-mediated currents were recorded at -70 mV holding potential. Then, NMDA receptor-mediated currents at -40 mV holding potential. Between the change in holding potential adequate time passed for the membrane potential to stabilize (3-5 min). The AMPA receptor-mediated current peak was quantified from currents recorded at -70 mV. At -70 mV NMDA receptors are blocked by Mg^{2+} ions. At +40 mV both NMDA and AMPA receptors are active. Since AMPA receptors have much faster kinetics, NMDA receptor-mediated current was quantified 30 ms after stimulation to assure adequate decay of the faster AMPA receptor-mediated current. Electrical stimulation was used to elicit action potentials in olfactory sensory neuron axons. Glass pipettes with an opening between 4-8 µm were filled with ACSF and placed in the olfactory nerve layer for stimulation. Currents at -70 mV and at +40 mV were recorded in the same mitral cell employing the same stimulation strength. AMPAR/NMDAR ratio was calculated by dividing the peak of the AMPA receptor-mediated current by the NMDA receptor-mediated current. Data was analyzed using PatchMaster.

2.3.8 Paired-pulse ratio

Gabazine (10 µM) and APV (50 µM) were added to the extracellular ACSF. The intracellular solution contained (in mM): 130 potassium gluconate, 10 Hepes, 10 phosphocreatine disodium salt hydrate, 10 sodium D-gluconate, 4 ATP magnesium salt, 4 NaCl, 0.3 GTP sodium salt hydrate, 1mM lucifer yellow CH, pH was adjusted with KOH to 7.2. Electrical stimulation was used to elicit action potentials in olfactory sensory neuron axons. Glass pipettes with an opening between 4-8 µm were filled with ACSF and placed in the olfactory nerve layer for stimulation. Two stimulations with a 20 Hz frequency were applied. Periglomerular cells were recorded at -70 mV holding potential. Data was analyzed using PatchMaster.

2.3.9 Excitation/Inhibition ratio

Electrical stimulation was used to elicit action potentials in olfactory sensory neuron axons. Therefore, glass pipettes with an opening between 4 to 8 µm were filled with ACSF and placed in the olfactory nerve layer. APV (50 µM) was added to the extracellular ACSF. The intracellular solution contained (in mM): 120 caesium gluconate, 10 CsCl, 10 Hepes, 10 phosphocreatine disodium salt hydrate**,** 8 NaCl, 2 ATP magnesium salt, 0.3 GTP sodium salt hydrate, 0.2 EGTA, pH was adjusted with CsOH to 7.3. An excitatory current was recorded at -70 mV holding potential. A composite (excitatory and inhibitory) current was recorded at -10 mV holding potential. The purely inhibitory current was calculated by first scaling the excitatory current recorded at -70 mV to the peak of the excitatory current of the composite current. Then this scaled excitatory current was subtracted from the composite current, which resulted in the purely inhibitory current. The inhibitory postsynaptic current (IPSC)/excitatory postsynaptic current (EPSC) ratio was calculated by dividing the peak of the purely inhibitory current by the peak of the excitatory component of the composite current. Data was analyzed with IgorPro 6.37 (WaveMetrics) using the Neuromatic and Patcher's Power Tools software packages.

2.3.10 Postsynaptic potentials

APV (50 µM) was added to the extracellular ACSF. The intracellular solution contained (in mM): 130 potassium gluconate, 10 Hepes, 10 phosphocreatine disodium salt hydrate, 10 **s**odium D-gluconate, 4 ATP magnesium salt, 4 NaCl, 0.3 GTP sodium salt hydrate, 5mM lidocaine-N-ethylbromide, pH was adjusted with KOH to 7.2. Electrical stimulation was used to elicit action potentials in olfactory sensory neuron axons. Glass pipettes with an opening between 4-8 µm were filled with ACSF and placed in the olfactory nerve layer for stimulation. Stimulation was set in current clamp to elicit a postsynaptic current with an amplitude of 100 pA to normalize input strength. Holding current in current clamp was set to stabilize the membrane potential at -50 mV before stimulation onset. A train of 10 stimuli with a 20 Hz frequency was applied. Data was analyzed using PatchMaster.

2.3.11 Action potential probabilities

APV (50 µM) was added to the extracellular ACSF. The intracellular solution contained (in mM): 130 potassium gluconate, 10 Hepes, 10 phosphocreatine disodium salt hydrate, 10 sodium D-gluconate, 4 ATP magnesium salt, 4 NaCl, 0.3 GTP sodium salt hydrate, pH was adjusted with KOH to 7.2. Electrical stimulation was used to elicit action potentials in olfactory sensory neuron axons. Glass pipettes with an opening between 4-8 µm were filled with ACSF and placed in the olfactory nerve layer for stimulation. Stimulation was normalized in current clamp to elicit a post synaptic current with an amplitude of 100 pA. Holding current in current clamp was set to stabilize the membrane potential at -50 mV. A train of 10 stimuli at a 50 Hz frequency was applied. Data was analyzed with IgorPro 6.37 (WaveMetrics, USA) using the Neuromatic and Patcher's Power Tools software packages.

2.4 Behavior

2.4.1 RFID-chip implantation

RFID-chips were injected in the neck folds of 3 to 4 month old mice two weeks before start of the behavior experiment. Mice were intraperitoneally injected with a Fentanyl (0.05 mg/kg body weight) (Janssen, Belgium), Midazilam (5 mg/kg body weight) (Hameln Pharma Plus, Germany) and Medetomidin (0.5 mg/kg body weight) (Alvetra, Germany) mixture as anesthetic. Adequate depth of anesthesia was confirmed by pedal and tail-pinch reflexes. A heating pad was used to maintain body temperature. Eyes were protected with ointment (Bepanthen). Part of the back (approximately 2 x 2 cm) was shaved and disinfected with 70% Ethanol. Lidocain (1 %, 200 µl) was applied as local anesthetic. A small incision was made by which the RFID injector (EURO ID, Germany) loaded with an RFID-chip (EURO ID, Germany) was inserted. The injector needle was pushed underneath the skin towards the neck fold and the RFID-chip was ejected. The wound was sewn closed. Anesthesia was antagonized with a mixture of Atipamezol (750 µg/kg body weight) (Prodivet pharmaceuticals S.A., Belgium), Flumazenil (0,2 mg/kg body weight) (Fresenius Kabi AG, Germany) and

Naloxon (120 µg/kg body weight) (Inresa Arzneimittel GmbH, Germany). The following 48 hours the mice received Carprofen (5 mg/kg body weight) (Norbrook Laboratories, United Kingdom) each 12 hours for pain reduction. The first night the cages were partly placed on a heating plate (37°C).

2.4.2 Automated behavior setup

The automated behavior setup described in Reinert *et al.* 2019 was used. The mice were housed in a group-housing cage containing enrichment. An elevated tunnel containing the olfaction port at which odorants and water reward were dispensed could be reached via a ramp. A dual channel olfactometer consisting of a central manifold and two channels with 10 odor reservoir connectors each was used to apply odors. Each odor was supplied randomly from one of at least two reservoirs to prevent learning of non-odor cues. IgorPro 6.37 (Wavemetrics, USA) was used to control and record the setup (Reinert *et al.* 2019).

2.4.3 Trial structure

Odor differentiation trials were structured according to Reinert *et al.* 2019. A schematic representation of the trial structure is shown in figure12. Mice initiated a trial by breaking two infra-red (IR) beams located in the odor port. After disruption of the IR beam the RFID chip was read. And in the next 500 ms the dwell rate (added fractions of time for broken IR beams: time IR beam broken/ 500 ms) was recorded and if it exceeded a threshold (1.75) the odor was presented for 2 s. Mice had to lick the water outlet more than 50% of the time in the 2 s after odor onset to be scored as expecting a reward. Only after a successful S^+ trial a water reward was dispensed (25 µl). To motivate the mice to perform correct trials an inter-trial interval (ITI) was introduced. The ITI was the time between trials in which the mouse was not able to initiate another trial by inserting its head into the odor port. ITIs were specific for each mouse: given that ITI is active for one mouse, another mouse can initiate a trial. If a mouse tried to initiate a trial, while its ITI was still running, the ITI was reset to the original duration. The ITI for successful trials was 1 s for unsuccessful trials 8 s.

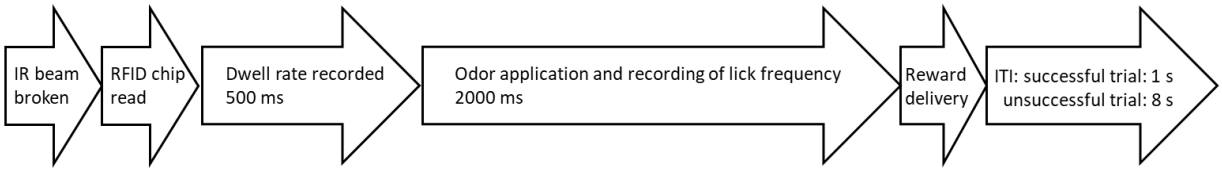

Figure 12: Trial structure of behavioral task. Abbreviation: ITI: inter-trial interval

2.4.4 Behavioral tasks

A go/no-go operant conditioning task was employed as described previously (Abraham *et al.* 2004). Mice were put into a group-housing cage without access to the elevated platform. Food and water were available *ad libitum* to acclimatize to the setup. After 24 h the water was removed and access to the elevated platform, on which the odor port was located, was granted. To teach the mice the trial structure a pretraining consisting of 7 stages with increasing difficulty was started. For each stage a minimal number of trials and/or a certain performance level had to be performed or reached, respectively. After completion of the last pretraining stage, which encompassed the complete trial structure, mice were trained to differentiate two pure odors (cis-3-Hexen-1-ol, 2-Octanone, 5 v/v %) to learn the principle of an odor differentiation task. In the next step the mice learned to differentiate between another odor pair (amyl acetate (Fluka, Germany), ethyl butyrate (Sigma-Aldrich, USA), 1 v/v %). All odors were diluted in mineral oil (Sigma-Aldrich, USA). To increase difficulty of the odor discrimination mice had to distinguish between mixtures of odors: 55% ethyl butyrate-45% amyl acetate vs. 45% ethyl butyrate-55% amyl acetate. For all odor discrimination tasks the animal were divided into two groups of nearly identical size. The only difference between the groups was which odor was the S^+ odor.

2.4.5 Setup control, data acquisition and analysis

The setup was controlled using IgorPro 6 (Wavemetrics, USA). Code was written by Janine Reinert and Prof. Dr. Andreas Schäfer. The software controlled the individualized behavior paradigm for each animal and recorded their behavioral responses. Data was analyzed partly with custom written code in IgorPro by Janine Reinert and partly with custom written code in R written by the author.

2.5 Computational OB model

The olfactory bulb model was adapted from Li & Cleland 2017 with support from Johanna Meichsner. The strength of the odor input was varied. The reduced excitability in periglomerular cells in CKAMP44$^{-/-}$ mice was modeled by reducing currents of the olfactory sensory neuron to periglomerular synapse and of the mitral cell to periglomerular cell synapse by 50%. R code to analyze firing rate after odor onset was written by the author.

2.6 Data analysis

Statistical analysis was performed using GraphPad Prism 6.0 (GraphPad Software, USA) unless otherwise mentioned. Plots were generated with Inkscape 0.92 according to template generated with GraphPad Prism.

Student's t-test or one-way ANOVA was used for normally distributed data. Not normally distributed data was analyzed using Mann-Whitney test or Kruskal-Wallis test. Repeated measure experiments (e.g. train stimulations) were analyzed using a two-way ANOVA. Shapiro-Wilk test was used to assess normal distribution of data.

Normally distributed data was plotted as mean and standard deviation unless otherwise mentioned. Not normally distributed data was plotted as median and interquartile range or boxplot.

3 Results

3.1 Expression of CKAMP44 in the olfactory bulb

In the first description of CKAMP44, von Engelhardt *et al.* showed that CKAMP44 mRNA is highly expressed in the olfactory bulb periglomerular layer, but not in the mitral and granule cell layer.

Because the periglomerular layer comprises several cell types with distinct properties, it is of interest which of these cells expresses CKAMP44. Therefore, I performed FISH co-staining against CKAMP44 mRNA and mRNAs of marker proteins. In order to identify single cells, I imaged with a comparably high resolution of 378 nanometer. As marker proteins, I selected CR, CB, GAD67 and TH, all of which show expression in the periglomerular layer (Kosaka & Kosaka 2007, figure 2). In addition, I compared the expression levels of CKAMP44 mRNA in the olfactory bulb with the expression in relay neurons of the LGN, in which CKAMP44 has a strong effect on AMPA receptor function (Chen *et al*. 2018).

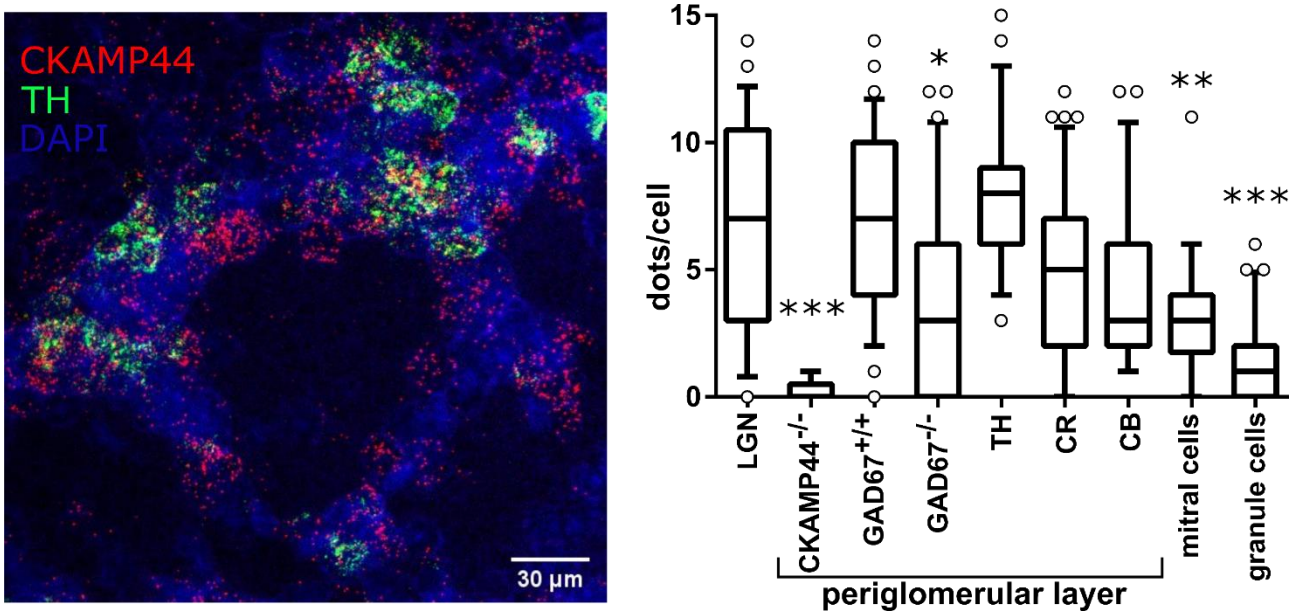

Figure 13: Fluorescent in situ hybridization. Double FISH stainings with a CKAMP44 probe and probes for mRNAs of selected marker proteins. Dots resulting from CKAMP44 probe per cell were quantified. Abbreviations: LGN: lateral geniculate nucleus, GAD67: glutamate decarboxylase, TH: tyrosine hydroxylase, CR: calretinin, CB: calbindin. N: LGN: 37, CKAMP44$^{-/-}$: 29, GAD67$^{+/+}$: 62, GAD67$^{-/-}$: 31, TH: 59, CR: 41, CB: 22, mitral cells: 34, granule cells: 30. All conditions were tested against mRNA level in the LGN serving as positive control: p-values: CKAMP44$^{-/-}$: < 0.001, GAD67$^{+/+}$: 1, GAD67$^{-/-}$: 0.018, TH: 0.9, CR: 0.36, CB: 0.22, mitral cells: 0.002, granule cells: < 0.001 .

The results show no significant difference in CKAMP44 mRNA level between the LGN and GAD67, TH, CR and CB expressing cells in the periglomerular layer. CKAMP44 levels in granule, mitral and periglomerular layer GAD67$^{-/-}$ cells were significantly lower than the LGN mRNA level. No CKAMP44 mRNA signal was detected in CKAMP44$^{-/-}$ mice, demonstrating the specificity of the CKAMP44 FISH signal.

3.2 Functional role of CKAMP44 in different olfactory bulb cell types

Considering the variability of CKAMP44 mRNA levels in the different cell types of the olfactory bulb, I assessed the influence of CKAMP44 deletion on AMPA receptor-mediated currents in multiple cell types. AMPA receptor-mediated currents were analyzed in the following cell types: periglomerular, external tufted, superficial short-axon, mitral and granule cells. mEPSCs were recorded in CKAMP44$^{-/-}$ mice and their wildtype littermates. Figure 14 shows amplitude and frequency of mEPSCs.
mEPSC peak amplitude and frequency were significantly reduced by 37% and 80%, respectively, in periglomerular cells of CKAMP44$^{-/-}$ mice. mEPSC peak amplitude was unchanged, but frequency was reduced by 46% in superficial short-axon cells of CKAMP44$^{-/-}$ mice. In mitral cells, external tufted cells and granule cells mEPSCs did not differ between CKAMP44$^{-/-}$ and wildtype mice.
Alterations in amplitude and frequency of AMPA receptor-mediated mEPSC can be caused by multiple mechanism (pre- and postsynaptic). To further investigate reasons for the change of AMPA receptor-mediated currents, I analyzed the ratio between AMPA receptor-mediated currents and NMDA receptor-mediated currents (AMPAR/NMDAR ratio). Results are shown in figure 15.

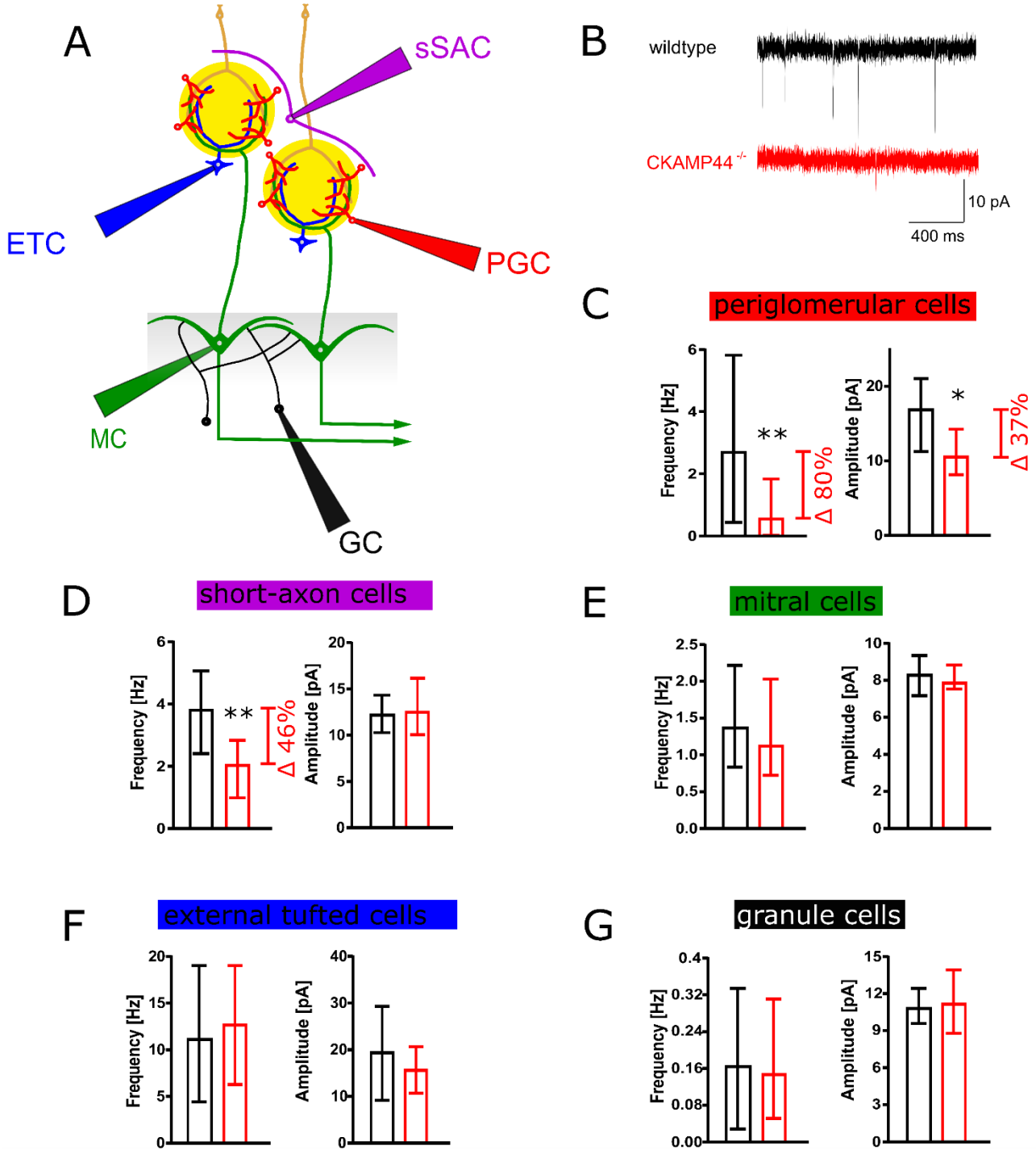

Figure 14: mEPSC recordings of CKAMP44$^{-/-}$ and wildtype mice in olfactory bulb neurons. A: schematic of recording configuration. B: Example traces of mEPSC recordings in periglomerular cells. C: mEPSC amplitude and frequency of periglomerular cells (PGC), D: mEPSC amplitude and frequency of superficial short-axon cells (sSAC), E: mEPSC amplitude and frequency of mitral cells (MC), F: mEPSC amplitude and frequency of external tufted cells (ETC), G: mEPSC amplitude and frequency of granule cells (GC). N and p-values: Periglomerular cells: N: 20, 23, p-value: amplitude:0.015 frequency: 0.0098; short-axon cells: N: 19, 32, p-value: amplitude:0.55 frequency: 0.0036; mitral cells: N: 28, 3, p-value: amplitude:0.74 frequency: 0.16; external tufted cells: N: 21, 22, p-value: amplitude:0.15 frequency: 0.41; granule cells: N: 32, 30, p-value: amplitude: 0.48 frequency: 0.99.

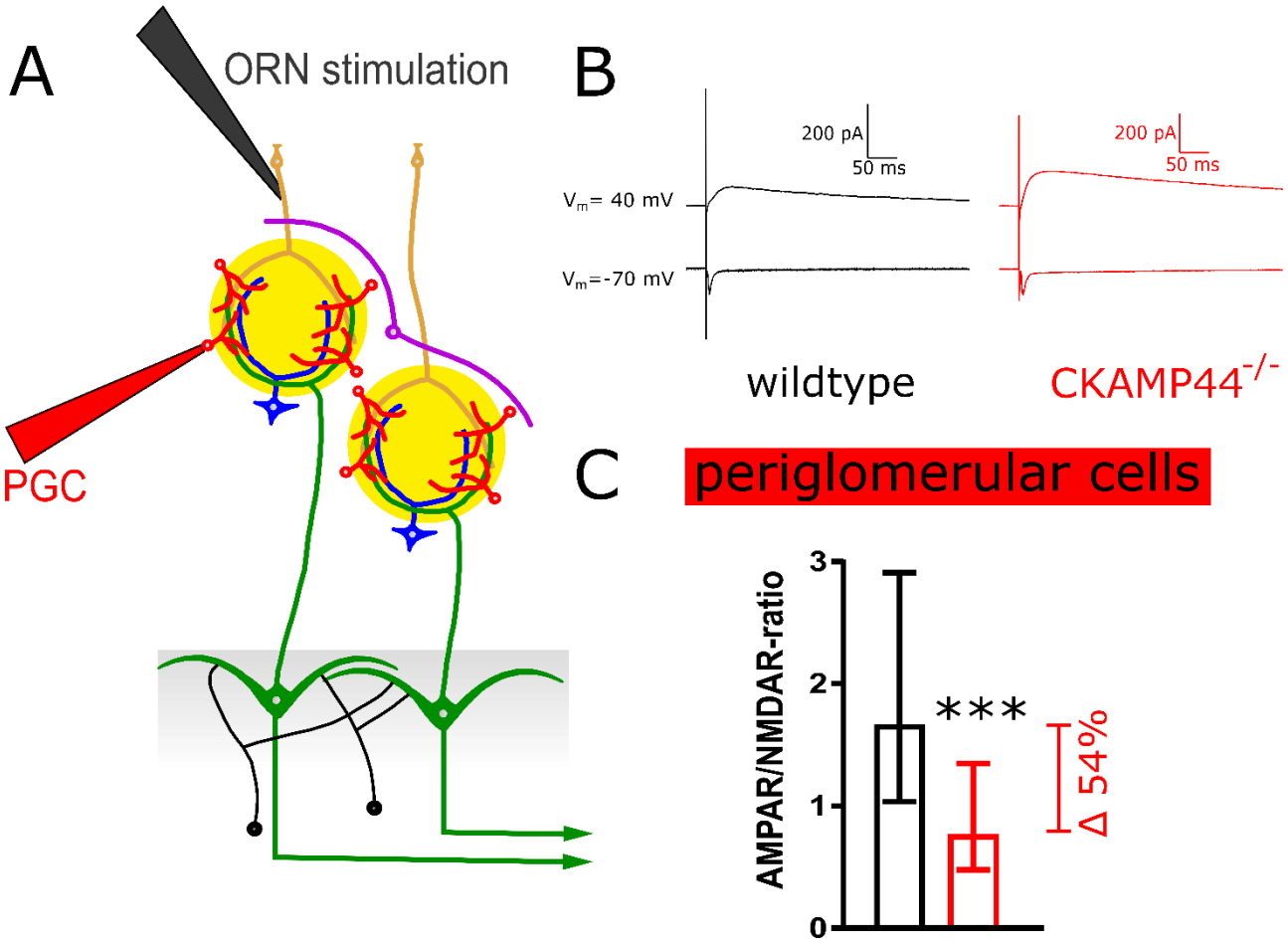

Figure 15: AMPAR/NMDAR ratio of periglomerular cells is reduced by CKAMP44 deletion. A: scheme of stimulation and recording configuration. B: example traces of currents recoded at 40 mV and -70 mV holding potential. C: AMPAR/NMDAR ratio quantification of CKAMP44$^{-/-}$ and wildtype mice. N: 23, 21; p-value: 0.0007.

The AMPAR/NMDAR ratio at the olfactory sensory neuron to periglomerular cell synapse was reduced by 54% in CKAMP44$^{-/-}$ mice in comparison to their wildtype littermates. Comparing the magnitudes of the reductions in AMPA-receptor mediated currents between mEPSC recordings and AMPAR/NMDAR ratios is challenging, since the absolute decrease of mEPSC amplitudes cannot be calculated, due to small mEPSCs that fall below the detection threshold. I employed amplitude event-count matching (Stell & Mody 2002) to approximately calculate the absolute changes for AMPA receptor-mediated current amplitudes in the mEPSC recordings (figure 16). This indicated that AMPA receptor-mediated current amplitudes are decreased in CKAMP44$^{-/-}$ mice by 51%, which is similar to the 54% decrease estimated from the reduced AMPAR/NMDAR ratio.

A

Amplitude calculation

Condition 1			Condition 2		
Cell 1	Cell 2	Cell 3	Cell 1	Cell 2	Cell 3
12	14	14	11	7	11
12	13	13	10	7	10
11	12	12	9	6	9
10	11	11	8	5	8
10	10	10	7	5	7
9	9	7	6		6
7	7	7	5		5
6	7	6			
4	6				
4	6				
8,5	9,5	10	8	6	8
9,3			7,3		
Δ 2					

EVENT COUNT MATCHING

Condition 1			Condition 2		
Cell 1	Cell 3	Cell 3	Cell 1	Cell 2	Cell 3
12	14	14	11	7	11
12	13	13	10	7	10
11	12	12	9	6	9
10	11	11	8	5	8
10	10	10	7	5	7
11	12	12	9	6	9
11,7			8		
Δ 3.7					

B

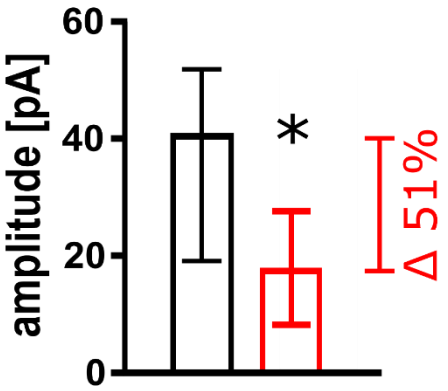

Figure 16: Calculation of magnitude of reduction of AMPA receptor-mediated currents in periglomerular cell mEPSC recordings. A: Tables show explanatory data to illustrate the principle of amplitude event count matching (Stell & Mody 2002). In the depicted explanatory data set the cell with the lowest number of mEPSCs has 5 events. Therefore, only the 5 largest mEPSC amplitudes per cell are used to calculate the mean amplitude. Means are highlighted in green. Differences between condition 1 and condition 2 are highlighted in red. B: Amplitude of periglomerular cell mEPSCs after event count matching. In my experiment the cell with the lowest number of mEPSCs in the recorded time window showed 16 mEPSCs (corresponding to the 5 mEPSC amplitudes shown in the explanatory data). Therefore, only the 16 largest mEPSCs in each cell were used to calculate the average amplitude. p-value: 0.0022.

It has been shown before, that CKAMP44 affects short-term plasticity in the hippocampus and thalamus (Khodosevich *et al.* 2014, Chen *et al.* 2018). To test whether CKAMP44 deletion alters short-term plasticity in periglomerular cells, I stimulated olfactory sensory neurons with paired-pulses. The results are shown in figure 17. The paired-pulse ratio in periglomerular cells of CKAMP44$^{-/-}$ mice did not differ from the paired-pulse ratio in wildtype littermates.

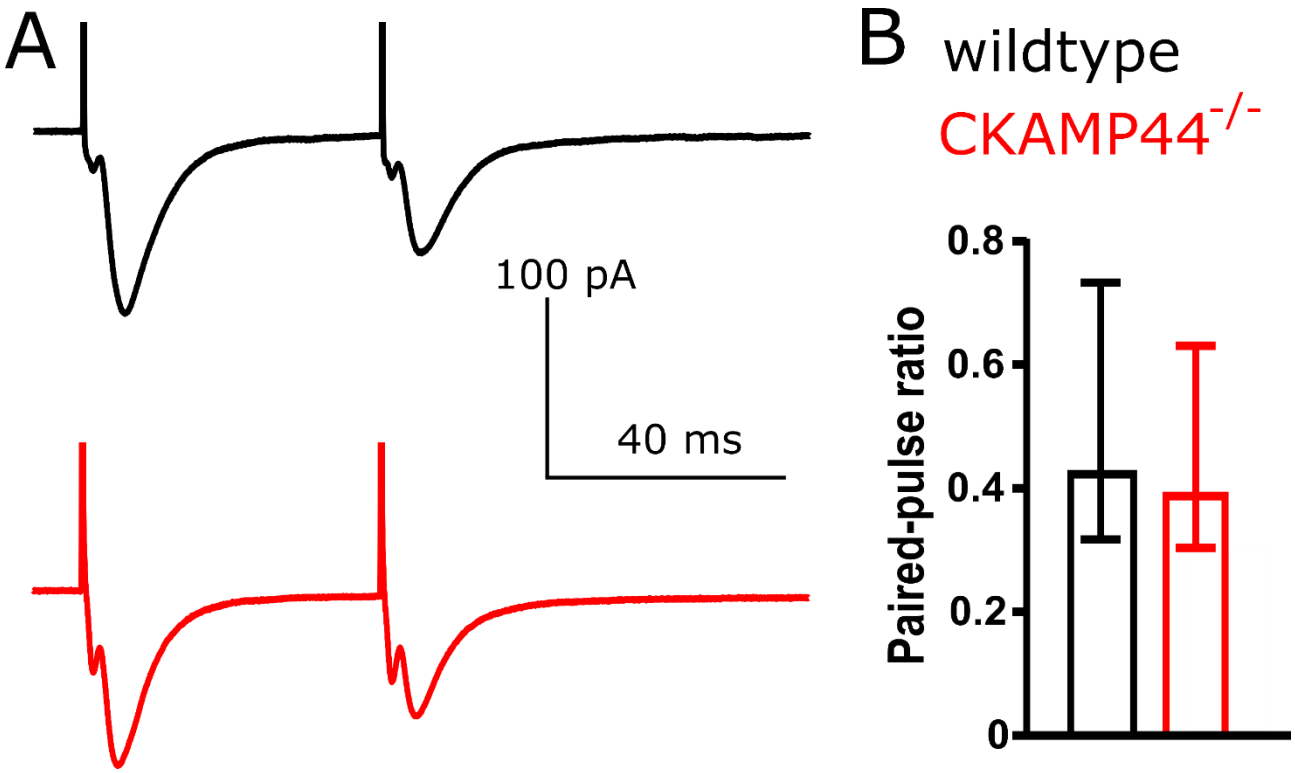

Figure 17: Short-term plasticity in the olfactory sensory neuron to periglomerular cell synapse is not affected by CKAMP44 deletion. A: Example traces of paired-pulse recording of periglomerular cells. Stimulus artefacts were cropped. B: Quantification of paired-pulse ratio of CKAMP44 and wildtype mice. N: 27, 34; p-value: 0.46.

3.3 Indirect effect of CKAMP44 on mitral cell activity

The previous experiments analyzed the direct effect of CKAMP44 on AMPA receptor-mediated currents in periglomerular cells. A reduced activation of periglomerular cells may affect feedforward inhibition onto mitral cells. As a next step, I therefore elucidated how the olfactory bulb network and especially the activity of mitral cells are affected by the observed decrease in AMPA receptor-mediated currents in periglomerular cells. I estimated changes in periglomerular cell inhibition onto mitral cells by quantifying the ratio of evoked IPSCs and EPSCs. Results and example traces are shown in figure 18.

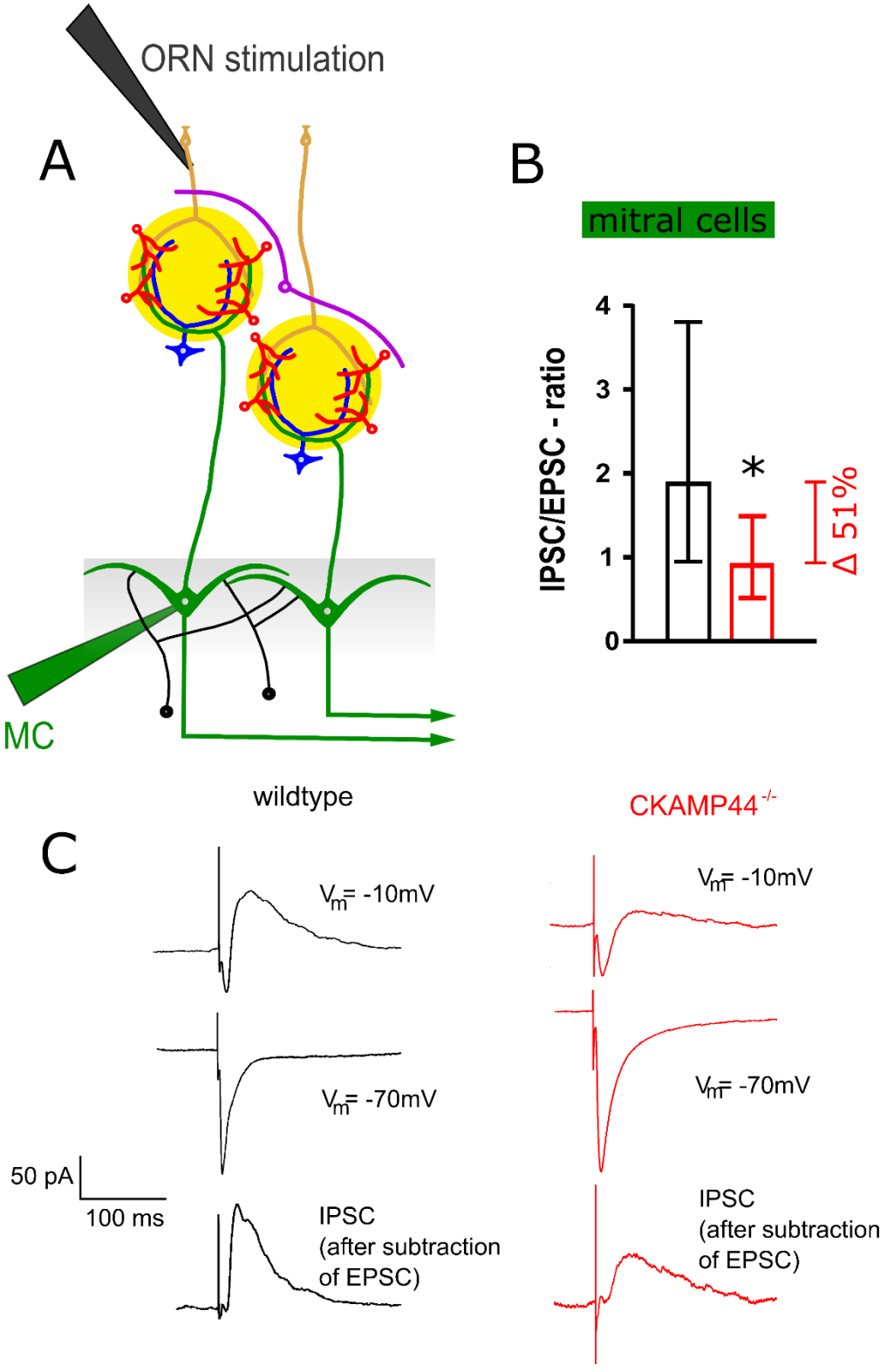

Figure 18: Recording of evoked IPSCs and EPSCs in mitral cells. A: Scheme of stimulation of olfactory sensory neurons and recording from mitral cells. B: Quantification of the IPSC/EPSC-ratio in CKAMP44$^{-/-}$ and wildtype mice. C: Example traces of composite (EPSC + IPSC) currents recorded at -10 mV (upper traces), EPSCs recoded at -70 mV (middle traces) and IPSCs (lower traces). IPSCs were calculated by subtracting amplitude-normalized EPSCs from the composite EPSC+IPSC currents. N: 29, 21; p-value: 0.018.

The IPSC/EPSC ratio was reduced by 51% in CKAMP44$^{-/-}$ mice when compared to wildtype mice. Given that CKAMP44 deletion did not affect mEPSC amplitude and frequency in mitral cells, the reduced IPSC/EPSC suggests that IPSC amplitude is decreased. This is consistent with a reduced feedforward inhibition from periglomerular cells in CKAMP44$^{-/-}$mice.

In the next experiment, I investigated whether the reduction on feedforward inhibition affects composite postsynaptic potentials (PSPs) in mitral cells of CKAMP44$^{-/-}$ mice. Current was injected into mitral cells to stabilize the membrane potential at -50 mV, close to their normal resting potential (Heyward *et al.* 2001). Voltage-dependent sodium channels were blocked using QX-314. Stimulation strength was standardized to evoke EPSCs with a 100 pA amplitude in voltage clamp at a -70 mV holding potential. PSPs resulted from stimulation of olfactory sensory neuron axons with a train of 10 stimuli at 20 Hz. Results are shown in figure 19.

This experiment showed a significant increase of PSP area under the curve (AUC) in mitral cells of CKAMP44$^{-/-}$ mice in comparison to their wildtype littermates. This is consistent with a reduced periglomerular cell feedforward inhibition and unaltered direct olfactory sensory neuron excitation of mitral cells.

In the next experiment, I investigated whether the reduced feedforward inhibition affects firing probability of mitral cells during excitation from olfactory sensory neurons. Recording and stimulation conditions were similar to the last experiments, except for the omission of voltage gated sodium channel block. Stimulation strength was standardized to evoke EPSCs with a 100 pA amplitude in voltage clamp at a -70 mV holding potential. Action potential probability (figure 20) was indeed increased in mitral cells of CKAMP44$^{-/-}$ mice in comparison to their wildtype littermates, consistent with a reduced feedforward inhibition from periglomerular cells.

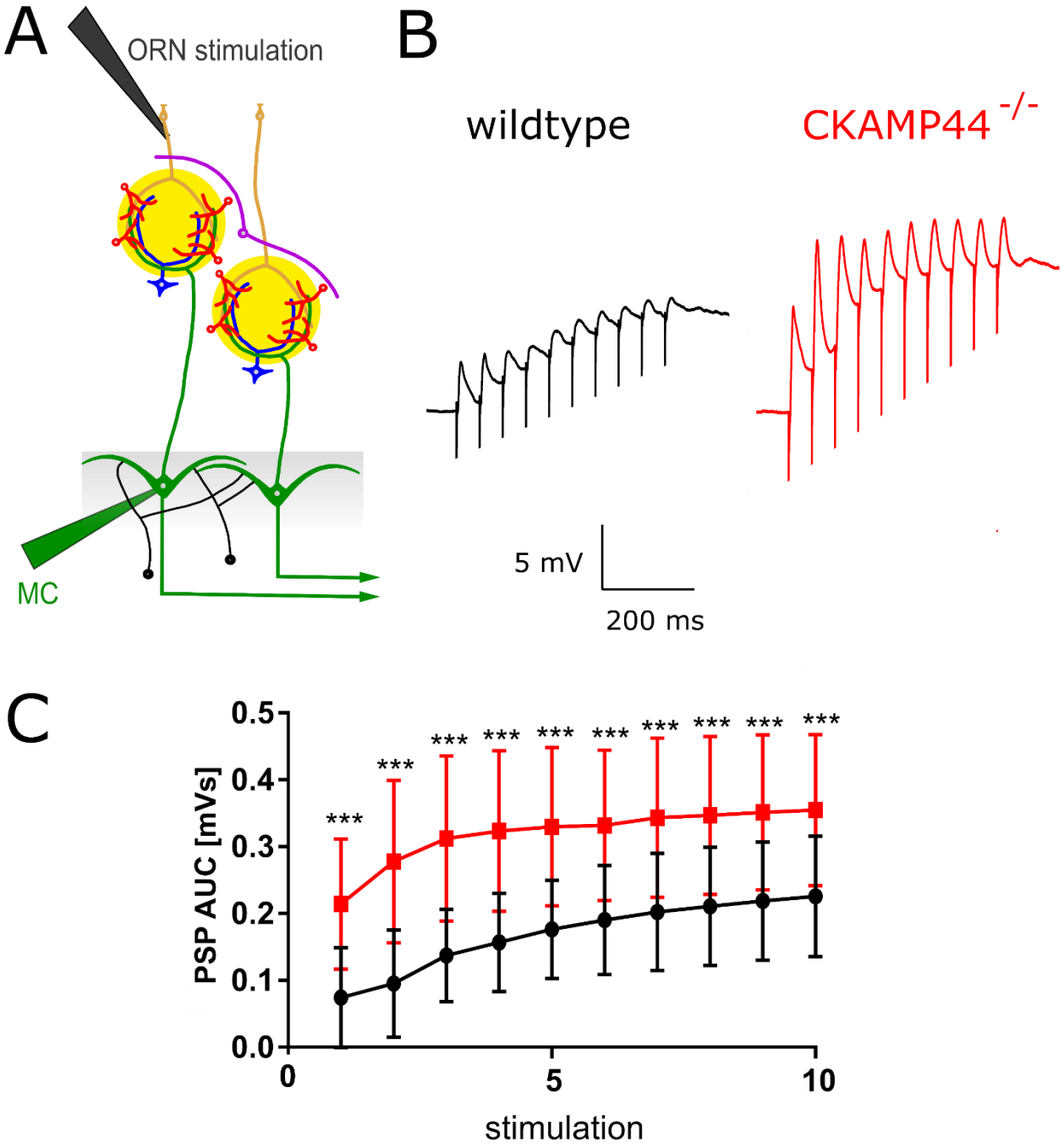

Figure 19: CKAMP44 deletion increases mitral cell PSPs. A: Scheme of stimulation and recording configuration. B: Example traces of PSPs from mitral cells of wildtype and CKAMP44$^{-/-}$ mice. Stimulation artefacts were clipped. C: Quantification of PSP area und the curve (AUC) after each stimulus. Abbr: PSP: postsynaptic potential. N: 25,23, p-values: 0.0007, <0.0001, <0.0001, <0.0001, <0.0001, <0.0001, <0.0001, 0.0001, 0.0001, 0.0003.

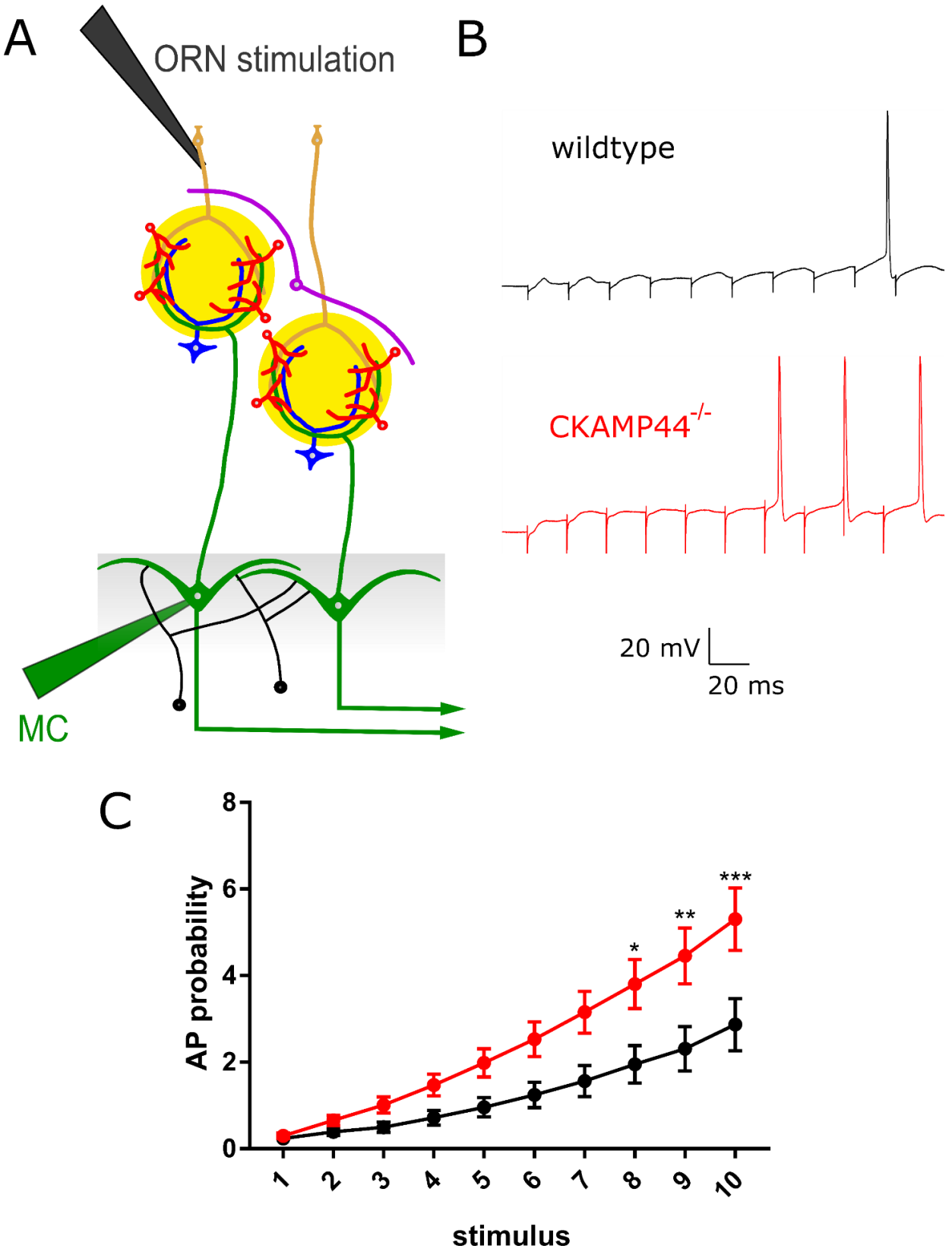

Figure 20: CKAMP44 deletion increases mitral cell action potential probability. A: Scheme of stimulation and recording configuration. B: Example traces of wildtype and CKAMP44$^{-/-}$ mice. C: Quantification of cumulative AP probability after each stimulus. AP: action potential. Mean and standard error of the mean were plotted. N: 27, 33; p-values: 0.99, 0.99, 0.98, 0.86, 0.52, 0.21, 0.05, 0.01, 0.0017, 0.0002.

3.4 Effect of CKAMP44 on odor discrimination ability

The described changes in network activity may affect olfactory bulb function. To assess changes in olfactory bulb function, I designed a behavior experiment in which CKAMP44$^{-/-}$ and wildtype mice had to distinguish between different odors. For this, I employed automated behavior testing. A recently published automated behavior box was used (Reinert *et al.* 2019). 22 mice were housed together in one cage and repeatedly performed a go/no-go odor discrimination task to obtain water. This approach had the advantage to reduce the stress level of the mice compared to conventional behavior experiments. Several factors contributed to this reduced stress level: Mice were tested in their home cage environment. Additionally, mice could choose the timing of the odor discrimination trials themselves. Experimenter interaction was minimized (Sorge *et al.* 2014).
Mice performed a simple and subsequently a difficult odor discrimination task. In the simple task, they differentiated between two pure odors, amyl acetate and ethyl butyrate. In the complex task, mice had to differentiate a 55% amyl acetate-45% ethyl butyrate mixture from a 45% amyl acetate-55% ethyl butyrate mixture. For the simple task the following parameters were considered:

- performance (percentage of correct trials)
- learning speed (trials until 80% criterion performance was achieved)
- discrimination time (time until head withdrawal in S$^-$ tasks)

For the complex task, only performance was considered. For the calculation of learning speed and discrimination time, mice had to achieve 80% criterion performance and many mice were not able to differentiate the mixtures at an adequate performance level. See figure 21 for results.

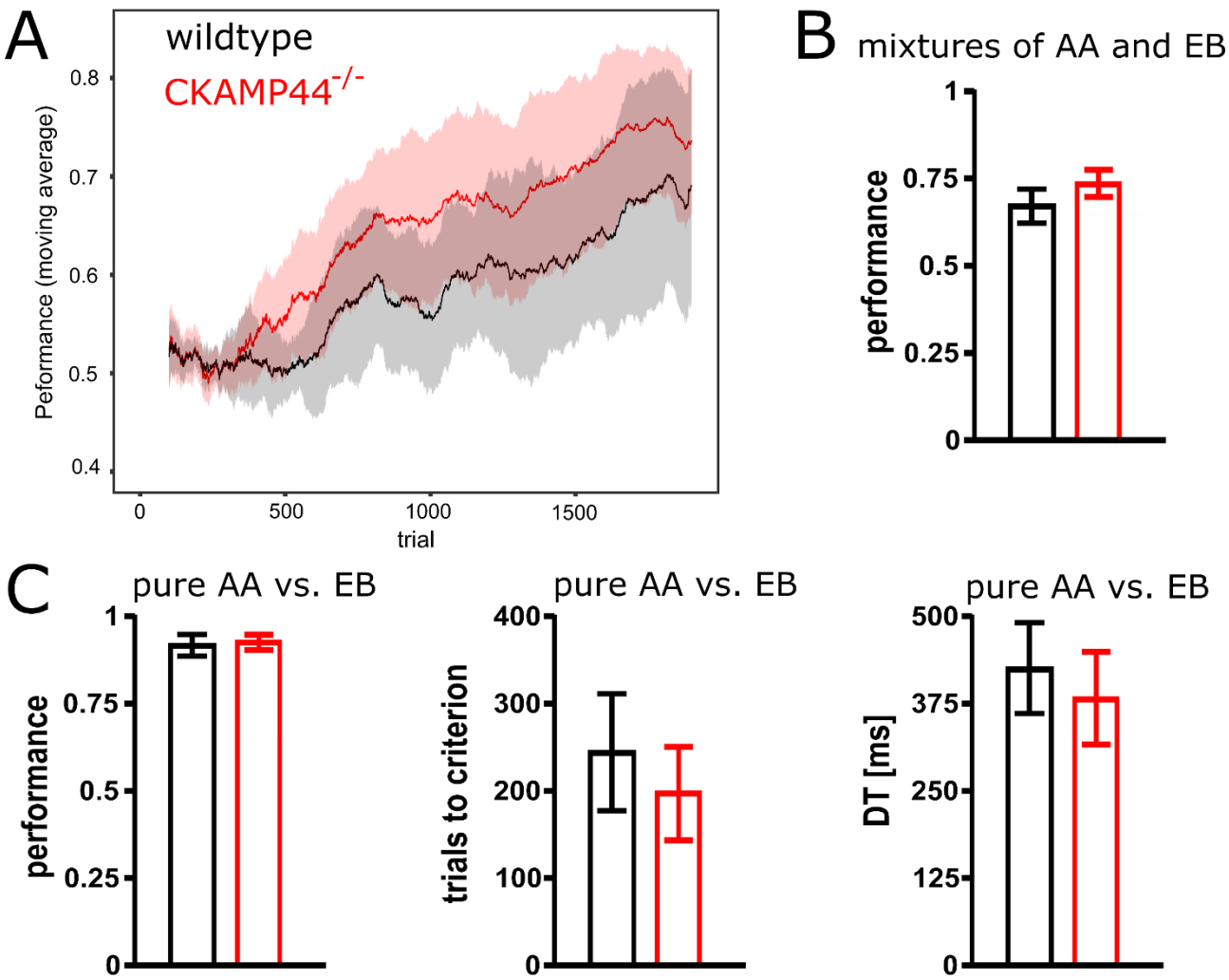

Figure 21: CKAMP44 deletion does not influence the ability of mice to differentiate between odors. A: Average traces of performance for differentiating between difficult mixtures. Plotted as sliding average over 200 trials. Shaded areas indicate standard deviation. B: Performance of CKAMP44$^{-/-}$ and wildtype mice differentiating difficult mixtures. C (left to right): Performance, learning speed and discrimination time of CKAMP44$^{-/-}$ and wildtype mice when differentiating pure amyl acetate vs. ethyl butyrate. Abbreviations: AA: amyl acetate, EB: ethyl butyrate, DT: discrimination time. N: 9, 13; p-values: performance (mixtures): 0.18, performance (pure odors): 0.30, trials to criterion (pure odors): 0.08, discrimination time (pure odors): 0.15.

The results show no reduction in the ability of CKAMP44$^{-/-}$ mice to differentiate between odors neither in easy nor in more challenging tasks. The speed of the odor discrimination as well as the learning speed was not affected in CKAMP44$^{-/-}$ mice, either.

3.5 Modeling the effect of CKAMP44 on olfactory bulb network activity

The previous experiments show that mitral cell activity was affected in CKAMP44$^{-/-}$ mice in *ex vivo* brain slices, but no CKAMP44 effect on odor behavior was observed. I employed an olfactory bulb network model to predict the effect of CKAMP44 deletion on mitral, periglomerular and granule cell activity to get additional information about how the olfactory bulb network could be affected. The olfactory bulb model published by Li & Cleland in 2017 was adapted with support from Johanna Meichsner. Periglomerular cell excitability was reduced to mimic the effect of CKAMP44 deletion observed in *ex vivo* slice electrophysiology experiments. Because it has been hypothesized that periglomerular cell function depends on the intensity of olfactory sensory neuron activity (Linster & Cleland 2009), the effect of CKAMP44 deletion was calculated for a spectrum of odor input concentrations. The model consists of 25 mitral cells and 25 periglomerular cells, which are paired to model for single glomeruli. 100 granule cells provide connections between individual glomeruli. Results see figure 22.

The adapted model predicted that a decreased periglomerular cell excitability increases mitral cell and granule cell firing frequencies in particular during weak odor input strength. With increasing olfactory sensory neuron activity, simulating a higher odor concentration, this difference was reduced. Since the excitability of periglomerular cells was reduced by 50%, the reduction in periglomerular cell activity was expected. The decreased periglomerular cell activity resulted in a reduced feed-forward inhibition from periglomerular cells onto mitral cells. This decreased inhibition together with an unchanged excitation caused the increase in mitral cell activity. Granule cell activity strongly correlated with mitral cell activity. This correlation resulted from the connectivity used in this model. The only inputs received by granule cells were excitatory inputs from mitral cells, therefore a higher mitral cell activity had to result in a higher granule cell activity.

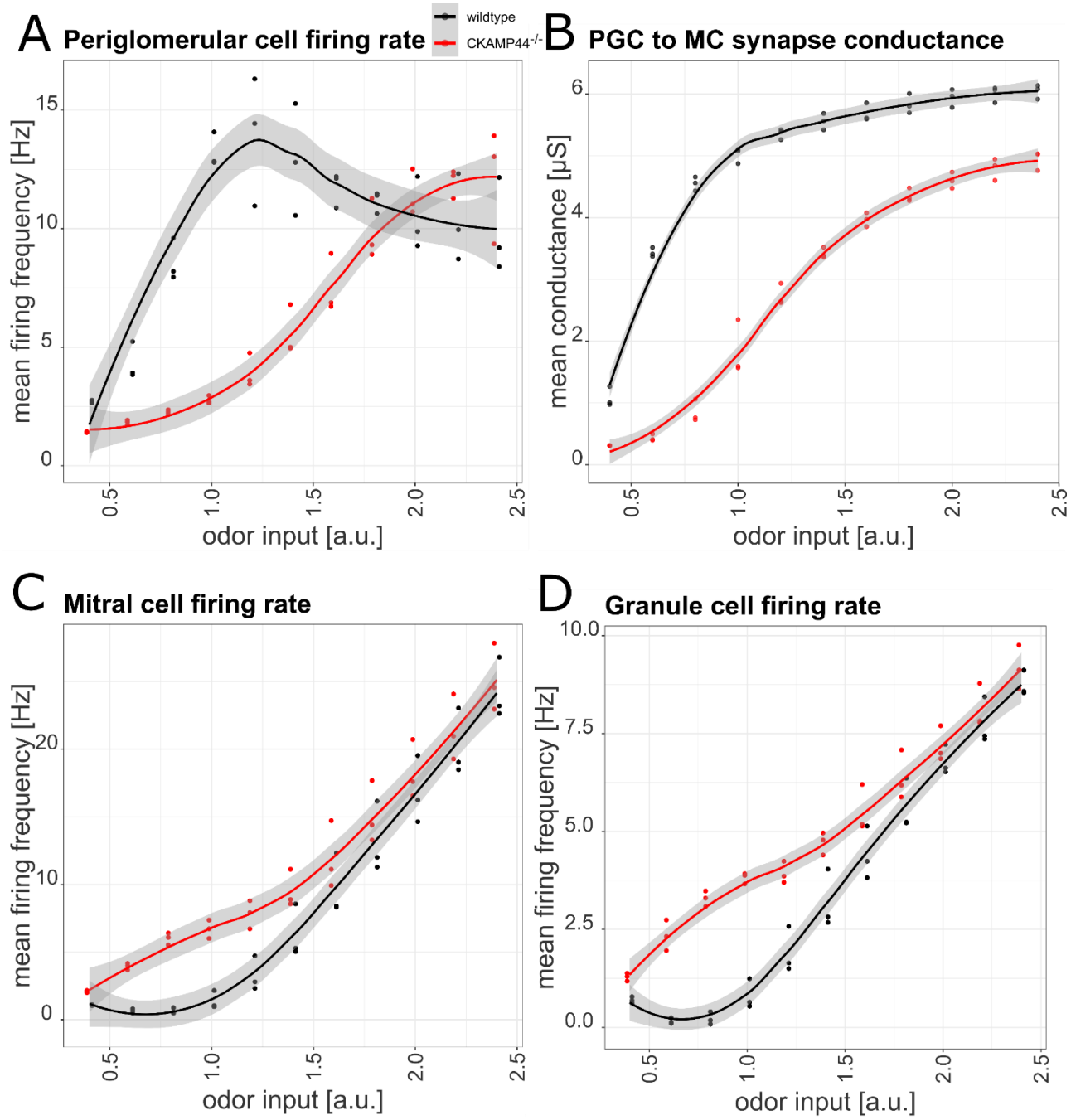

Figure 22: Model of effect of CKAMP44 deletion on olfactory bulb neuron firing rates depending on strength of olfactory sensory neuron input. A: Periglomerular cell firing rate B: Conductance at the periglomerular cell to mitral cell synapse C: Mitral cell firing rate D: Granule cell firing rate.

4 Discussion

The aim of this study is to elucidate the impact of CKAMP44 on the olfactory bulb network. To achieve this aim, I employed the following approach:

1. Identify the olfactory bulb cell types in which CKAMP44 exerts the strongest effect on AMPA receptor-mediated currents:
   Deletion of CKAMP44 reduced AMPA receptor-mediated currents mainly in periglomerular cells, but not in mitral cells.
2. Investigate mitral cell excitation and inhibition by activating the olfactory bulb network. Since AMPA receptor function is not altered in mitral cells of CKAMP44$^{-/-}$ mice, all observed changes are due to altered network inputs:
   Olfactory sensory neuron stimulation caused a higher activity of mitral cells, if CKAMP44 was deleted.
3. Investigate if olfactory bulb function is impaired *in vivo*. To this end, I tested whether CKAMP44 deletion affects the ability of mice to differentiate between different odors:
   CKAMP44 deletion did not influence odor differentiation under the applied test conditions.

4.1 CKAMP44 affects AMPA receptor-mediated currents in olfactory bulb cell types

As a first step, I identified which olfactory bulb cell types express high levels of CKAMP44 mRNA, as AMPA receptor-mediated currents of these cells are likely to be affected by CKAMP44 deletion. Hence, I performed double FISH stainings with CKAMP44 probes together with probes of marker proteins that have been shown to be expressed in the glomerular layer of the olfactory bulb (Kosaka & Kosaka 2007). Results showed a high expression of CKAMP44 mRNA in GABAergic, TH, CR and CB expressing cells (figure 13). These cells are mostly periglomerular cells together with a subpopulation of superficial short-axon cells (Nagayama *et al.* 2014). The CKAMP44 mRNA expression in these cells was similar to the expression in LGN relay

neurons, in which CKAMP44 deletion was shown to affect AMPA receptor-mediated currents (Chen *et al.* 2018). Mitral cells, in contrast to periglomerular cells, show a low expression of CKAMP44 mRNA (figure 13). Considering that mitral cells are bigger and have a far more elaborate dendritic arbor with more synapses than periglomerular cells (Price & Powell 1970, Pinching & Powell 1971), it is likely that mitral cells express more AMPA receptors than periglomerular cells, but a considerably lower percentage of these receptors are in a complex with CKAMP44. CKAMP44 mRNA FISH signal was nearly absent in granule cells, indicating that AMPA receptor-mediated currents are not affected in these cells.

To investigate whether CKAMP44 affects AMPA receptor-mediated currents as predicted from the FISH data, I recorded mEPSCs in the different cell types of CKAMP44 deficient and control mice. mEPSCs are independent from network activity, since action potential generation is pharmacologically prevented by blocking voltage-gated sodium channels with tetrodotoxin.

Amplitude and frequency of mEPSCs were quantified to assess changes in synaptic AMPA receptor number and function (figure 14). CKAMP44 deletion caused a strong reduction in frequency (reduced by 80 %) and amplitude (reduced by 37 %) of AMPA receptor-mediated mEPSCs in periglomerular cells. This finding matches the FISH data, which showed that periglomerular cells have a high CKAMP44 expression.

mEPSCs amplitude was reduced by 37% in superficial short-axon cells of CKAMP44$^{-/-}$ mice in comparison to wildtype littermates leading to the conclusion that CKAMP44 deletion reduces AMPA receptor-mediated currents in superficial short-axon cells as well, but to a lesser extent than in periglomerular cells. This fits to the FISH data, which show a high CKAMP44 mRNA expression in TH and GABAergic cells. A subpopulation of superficial short-axon cells expresses TH and GAD67 (Kiyokage *et al.* 2010). Therefore, CKAMP44 deletion might only affect a subpopulation of superficial short-axon cells. This subpopulation conveys interglomerular inhibition (Kiyokage *et al.* 2010, figure 6).

mEPSCs of granule cells, mitral cells and external tufted cells were not affected by CKAMP44 deletion. Neither mEPSC amplitude nor frequency was influenced by CKAMP44 deletion. All three cell types showed CKAMP44 mRNA levels significantly lower than the CKAMP44 mRNA level in periglomerular cells or relay neurons of the LGN.

Summing up, CKAMP44 mRNA expression is highest in periglomerular cells and a subpopulation of superficial short-axon cells. Deletion of CKAMP44 also has the strongest impact on AMPA receptor-mediated currents in periglomerular cells, only mildly affects those in superficial short-axon cells and has no effect on currents in mitral, external tufted and granule cells (figure 23). Similarly, Khodosevich *et al.* 2014 and Chen *et al.* 2018 found that CKAMP44 deletion alters AMPA receptor function significantly in cell types that show high CKAMP44 mRNA expression in wildtype mice. This suggests, that CKAMP44 protein levels correlate with the quantified CKAMP44 mRNA levels.

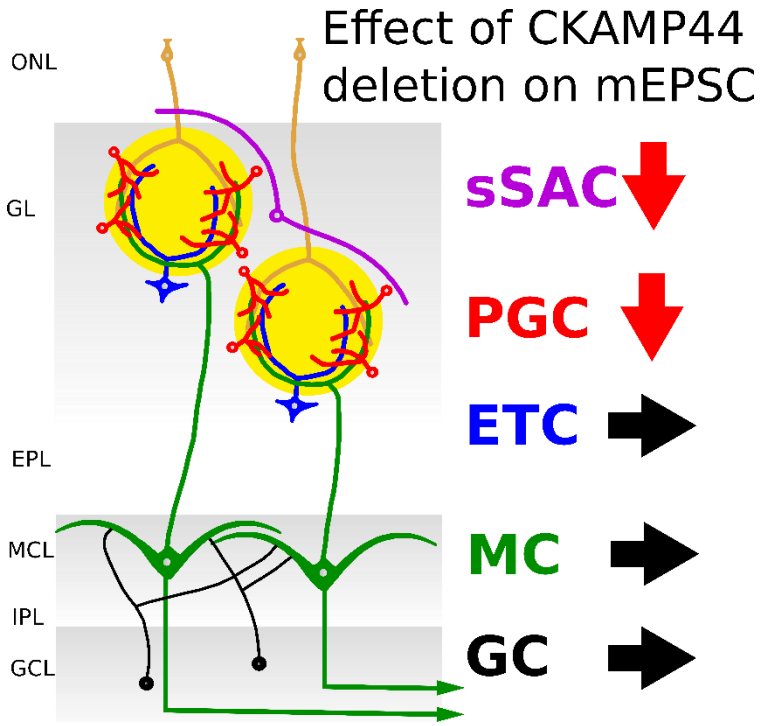

Figure 23: Changes due to CKAMP44 deletion in AMPA receptor-mediated mEPSCs in different olfactory bulb cell types. Abbreviations of layers is given on the left and cell types legend is color coded on the right. Black horizontal arrows indicate no changes. Red downward arrows indicate decreased AMPA receptor mediated currents due to CKAMP44 deletion. ONL: olfactory nerve layer, GL: glomerular layer, EPL: external plexiform layer, MCL: mitral cell layer, IPL: internal plexiform layer, GCL: granule cell layer, PGC: periglomerular cell, sSAC: superficial short-axon cell, ETC: external tufted cell, MC: mitral cell, GC: granule cell

To get a better estimate about the magnitude of the reduction of AMPA receptor-mediated current amplitudes, I quantified AMPAR/NMDAR ratios. Based on this analysis, AMPA receptor number is approximately reduced by 54% in olfactory

sensory neuron to periglomerular cell synapses of CKAMP44$^{-/-}$ mice (figure 15). This approximation is made under the assumption that NMDA receptors are not affected by CKAMP44 deletion. Even though the findings of changes in AMPA receptor-mediated currents are qualitatively the same in mEPSC recordings and AMPAR/NMDAR ratio analysis, the quantitative change seems to differ. AMPAR/NMDAR ratios were reduced by 54% compared to an 80% reduction in mEPSC frequency and 37% reduction in mEPSC amplitude. Changes in mEPSCs are hard to reliably quantify since a reduction in amplitude leads to a reduction in frequency due to events falling below the detection limit. One approach to solve this challenge is an amplitude event count matching procedure published by Stell & Mody in 2002. This method was originally developed for an experiment with different preconditions. As a consequence, it is based on several assumptions that are not necessarily given in my mEPSC recordings. The most significant assumption is that any reduction in frequency is due to a reduction in amplitude, which causes events to fall below the detection threshold. In figure 16 a visual explanation of the method is provided. The number of events in the low frequency condition is matched to the same number of events in the high frequency condition with the highest amplitude. The idea behind this operation is, that events recorded in the low frequency condition correspond to events with the highest amplitude recorded in the high amplitude condition. All additional events in the high frequency condition occur in the low frequency condition as well, but are not detected because they fall below the detection threshold. For the remaining events (all events of the low frequency condition and the same number of events from the high frequency condition selected for the highest amplitude), the amplitude is calculated to return the true difference in current strength between conditions. Applying this method to the mEPSC data results in a reduction of 51% in AMPA receptor-mediated current amplitudes due to CKAMP44 deletion. This 51% reduction is similar to the 54% reduction observed in the AMPAR/NMDAR recordings.

The similarity between the results obtained from evoked and spontaneous currents is an indication that the previously discussed assumptions are met. Nevertheless, it is also possible that the reduction in evoked AMPA receptor-mediated currents differs from the reduction in amplitudes of spontaneous events, because different and partially non-overlapping synapses are analyzed in AMPAR/NMDAR ratio experiment and mEPSC recordings. For example, the mitral cell to periglomerular cell synapse might be affected differently than the olfactory sensory to periglomerular cell synapse

(only the latter was investigated in AMPAR/NMDAR ratio experiment). One possible explanation why synapses might be differentially affected is that type-I periglomerular cells form synapses mainly with olfactory sensory neurons and mitral cells, while type-II periglomerular cells form synapses with mitral and external-tufted cells (Kosaka *et al.* 1998, Shao *et al.* 2009, Kiyokage *et al.* 2010). Additionally, it cannot be excluded that NMDA receptor-mediated currents might also change in CKAMP44$^{-/-}$ mice. However, this is unlikely as in other brain regions no indication that CKAMP44 deletion affects NMDA receptor-mediated current was found (Chen *et al.* 2018). Taken together, the experiments showed an approximately 50% decrease of AMPA receptor-mediated currents in periglomerular cells in CKAMP44$^{-/-}$ mice in comparison to wildtype mice.

Periglomerular cells type-I and type-II might be differently affected by CKAMP44 deletion. Excitability of periglomerular cells type-I is certainly reduced by deletion of CKAMP44, since AMPA receptor-mediated currents evoked by olfactory sensory neuron stimulation are reduced by CKAMP44 deletion and only type-I cells form synapses with olfactory sensory neurons (Kosaka *et al.* 1998). AMPA receptor-mediated currents in type-II periglomerular-cells, are likely also reduced by CKAMP44 deletion, considering that FISH data showed that type-I periglomerular cells (GABAergic and TH expressing cells according to Kosaka *et al.* 1996, 1998) as well as type-II periglomerular cells (CB and CR expressing cells according to Kosaka *et al.* 1996, 1998) had CKAMP44 mRNA levels not significantly different from CKAMP44 mRNA levels observed in LGN relay neurons.

CKAMP44 affects short-term plasticity in the dentate gyrus and the LGN (Khodosevich *et al.* 2014, Chen *et al.* 2018). Therefore, I analyzed the effect of CKAMP44 deletion on short-term plasticity at the olfactory sensory neuron to periglomerular cell synapse. Interestingly, CKAMP44 did not affect short-term plasticity at this synapse (figure 17). CKAMP44 deletion affects short-term plasticity in the dentate gyrus and LGN by increasing the rate of recovery from desensitization of AMPA receptors. Consequently, CKAMP44 deletion only affects short-term plasticity at synapses at which the rate of AMPA receptor recovery from desensitization influences short-term plasticity (Khodosevich *et al.* 2014, Chen *et al.* 2018). AMPA receptor desensitization often influences short-term plasticity at synapses with high release probability (Koike-Tani *et al.* 2008, Regehr 2012). The olfactory sensory neuron to periglomerular cell synapse

has a high release probability of approximately 0.8, yet short-term plasticity seems to be independent from AMPA receptor desensitization (Murphy *et al.* 2004). Two experiments performed by Murphy *et al.* support this theory. Cyclothiazide, which eliminates AMPA receptor desensitization (Yamada & Tang 1993), does not affect the paired-pulse ratio; and AMPA and NMDA receptor-mediated currents show a very similar paired-pulse depression. Short-term plasticity at the olfactory sensory neuron to periglomerular cell synapse is likely controlled by a reduced glutamate release at the presynapse (Murphy *et al.* 2004). The independence of short-term plasticity from AMPA receptor desensitization explains the lack of effect of CKAMP44 deletion on short-term plasticity at the olfactory sensory neuron to periglomerular cell synapse.

Employing electrophysiological analysis of the effect of CKAMP44 on AMPA receptor-mediated currents in combination with CKAMP44 mRNA expression analysis, I was able to identify cell types in the olfactory bulb network that are influenced by the AMPA receptor auxiliary subunit CKAMP44.

AMPA receptor-mediated currents in periglomerular cells are strongly affected by CKAMP44 deletion. In contrast, AMPA receptor-mediated currents in mitral cells are not affected by CKAMP44 deletion. I further showed that AMPA receptor function is mildly affected by CKAMP44 deletion in superficial short-axon cells. Granule and external tufted cells were, similar to mitral cells, not affected by deletion of CKAMP44.

These insights into the effect of CKAMP44 on AMPA receptor function in the respective cell types enable me to analyze the indirect effect of CKAMP44 on mitral cell activity in the next step.

4.2 Indirect influence of CKAMP44 on mitral cell activity

In the next step of this study, I analyzed if mitral cells are affected indirectly by the increased excitability of periglomerular cells in CKAMP44$^{-/-}$ mice. I investigated periglomerular cells and mitral cells in more detail for several reasons:

1. Excitability of periglomerular cells is affected by deletion of CKAMP44.
2. Excitability of mitral cells is unaltered by deletion of CKAMP44. Consequently, any changes in mitral cell activity are likely caused by network effects.

3. As principal output-neurons of the olfactory bulb, mitral cells play a significant role in information processing.
4. Intraglomerular feedforward and feedback mechanisms between periglomerular and mitral cells are hypothesized to be relevant for decorrelation (Linster & Cleland 2009).

To investigate network activity, I stimulated axons of olfactory sensory neurons and observed mitral cell activity in multiple experiments. In the first experiment, I recorded inhibitory and excitatory currents in mitral cells. Based on mEPSC data, I considered AMPA receptor-mediated currents in mitral cells as unchanged by the deletion of CKAMP44. Results show a reduction in IPSC/EPSC ratio caused by CKAMP44 deletion of 51% (figure 18). This indicates that the reduced excitatory drive of periglomerular cells translates into a reduced inhibition from periglomerular to mitral cells. Hence, expression of CKAMP44 directly affects network communication in the olfactory bulb.

In the next experiment, I tested if the decreased feedforward inhibition onto mitral cells affects compound PSPs. Olfactory sensory neurons were stimulated in a manner mimicking their *in vivo* activity. The PSP AUC increased more strongly in CKAMP44$^{-/-}$ mice than in wildtype mice (figure 18). This indicates that the deletion of CKAMP44 results in increased excitation of mitral cells due to the decreased inhibition from periglomerular cells. Importantly, also action potential frequency was increased in CKAMP44$^{-/-}$ mice when stimulating olfactory sensory neurons (figure 20).
These data support the hypothesis that the decreased excitability of periglomerular cells translates into an increased activity of mitral cells. Hence, network activity in the olfactory bulb is affected by CKAMP44. Moreover, it reveals the relevance of inhibition from periglomerular cells for mitral cell activity.
The question remains, if this changed mitral cell activity influences olfactory bulb function.

4.3 Influence of CKAMP44 on olfactory bulb function

A precise way to reliably assess olfactory bulb function is to analyze odor behavior. Thus, I tested the ability of CKAMP44$^{-/-}$ and wildtype mice to differentiate pure odors.

None of the tested parameters (discrimination time, performance or learning speed) were affected by CKAMP44. In a more difficult odor discrimination experiment, in which mixed instead of pure odors were employed, performance was assessed, which was also not affected by CKAMP44. Therefore, odor discrimination seems to be unaffected by CKAMP44.

Several factors could contribute to the fact that CKAMP44 did not show an effect on olfactory behavior. Mice carried a constitutive CKAMP44 deletion. The constitutive nature of the deletion increases the likelihood of compensatory changes during development that rescue olfactory bulb function. These changes could take place in the olfactory bulb itself or also in downstream brain regions. Considering the substantial ability of neuronal networks to compensate for changed network dynamics this is not an unlikely scenario. Some humans can smell and can differentiate between odors even without apparent olfactory bulbs (Weiss *et al.* 2020).

Another possibility is that the olfactory bulb function is perturbated only under certain conditions. Olfactory bulb function might only be affected in different tasks than those tested in this study. Periglomerular cells, which are most strongly affected by CKAMP44 deletion, might influence other functions of the olfactory bulb more strongly than odor discrimination. They might, for example, influence odor detection threshold. Alternatively, odor discrimination could be affected only at certain odor concentrations.

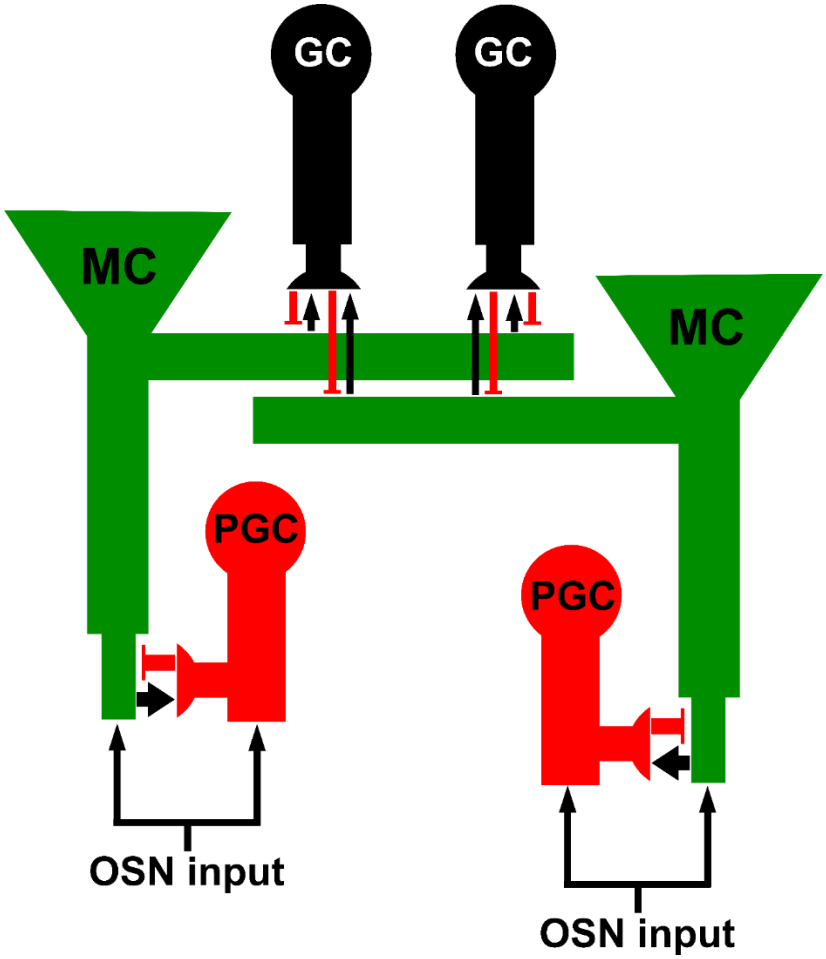

Figure 24: Architecture of adapted model. Periglomerular cells (PGCs) for reciprocal dendrodentritic synapses with one mitral cell (MC) each. Granule cells (GCs) form dendrodentritic synapses with multiple mitral cells. Red lines indicate inhibition and black arrows excitation. Figure adapted from Li and Cleland 2017.

Indeed, a computational olfactory bulb model adapted from Li and Cleland (2017) suggests that deletion of CKAMP44 affects periglomerular cell and mitral cell activity only under certain conditions. The connectivity employed in the model is shown in figure 24. Modeling predicts CKAMP44 deletion to decrease periglomerular cell activity and increase mitral and granule cell activity (figure 22).

Interestingly, mitral cell firing was only reduced in the lower to medium range of simulated input strength. This indicates that periglomerular cells are relevant to differentiate odors in particular at low odor concentrations. This might explain why no difference was observed in the odor differentiation experiment in which odor concentrations of 1% v/v were used. The computational model suggests that periglomerular cell activity does not reduce mitral cell activity at odor concentrations that are several orders of magnitude above the detection threshold.

A model can of course give no definite information about network activity *in vivo*. Therefore, olfactory bulb neuron activity would have to be measured *in vivo* in response to odors at different concentrations to further investigate the influence of CKAMP44 on olfactory bulb network activity. Mitral cell ensemble activity could be analyzed using two photon Ca^{2+}-imaging. This would for example allow me to assess whether CKAMP44 deletion and changes in periglomerular cell activity affect sparsity of mitral cell ensemble activity as predicted by computational models (Cleland & Linster 2005). Ensembles encoding different odors can be compared and the degree of similarity can be used to assess efficiency of decorrelation (Mazor & Laurent 2005).

Odor discrimination at the tested odor concentration is not affected by CKAMP44 deletion, even though mitral cell activity is increased. Therefore, decorrelation of odor information is still adequate in CKAMP44$^{-/-}$ mice even with reduced excitatory drive of periglomerular cells. Decorrelation of olfactory sensory input equals contrast enhancement, which means that the output, mitral cell activity, is sparser than the input, olfactory sensory neuron activity. Non-topographic contrast enhancement is necessary since odor molecules form a complex discontinuous distribution which is impossible to project onto the two-dimensional spaces formed by glomeruli or mitral cells (Linster & Cleland 2009). Periglomerular cells are hypothesized to play a role in contrast enhancement (Cleland & Sethupathy 2006).

Periglomerular cells type-I and type-II might differently affect contrast enhancement and be differently affected by CKAMP44 deletion as discussed earlier. The feed-forward and feedback inhibition of type-I periglomerular cells onto mitral cells is considered a fundamental part of contrast enhancement (Kosaka *&* Kosaka 2004, Cleland & Sethupathy 2006, figure 4). Periglomerular cells are activated and reach their maximum activity at lower olfactory sensory neuron input strength than mitral cells, due to their higher input resistance (Chen *et al.* 2002, Shen *et al.* 1999). Therefore, mitral cells receiving low olfactory sensory neuron input are more strongly affected and sometimes completely silenced by periglomerular feedforward inhibition than mitral cells receiving strong olfactory sensory neuron input. Therefore, only mitral cells innervated by olfactory sensory neurons with high affinity to the odor are activated. Mitral cells innervated by olfactory sensory neurons with lower affinity to the odor are inhibited due to periglomerular feedforward inhibition. This leads to contrast enhancement (Cleland & Sethupathy 2006). Therefore, the reduced inhibition of mitral

cells by periglomerular cells due to CKAMP44 deletion potentially impairs contrast enhancement.

Type-II periglomerular cells receive input from mitral and external tufted cells (Kosaka *&* Kosaka 2004, Shao *et al.* 2009). Both external tufted and mitral cells are activated at higher olfactory sensory neuron input strength than periglomerular cells type-I (Chen *et al.* 2002, Shen *et al.* 1999, Hayar *et al.* 2004). Therefore, type-II periglomerular cells inhibit mitral cells at higher sensory neuron input strength than type-I periglomerular cells and therefore likely affect contrast enhancement differently. The role of type-II neurons in olfactory bulb function is not well investigated, since most computational models as well as the model adapted in this study only include type-I periglomerular cells (Li & Cleland 2017, Cleland & Sethupathy 2006, Gilra & Bhalla 2015). Thus, the effect on olfactory bulb function of a reduced excitatory drive in type-II periglomerular cells due to CKAMP44 deletion might differ from the effect of type-I periglomerular cells.

mEPSC data shows that CKAMP44 deletion affects AMPA receptor function not only in periglomerular cells but also in superficial-short axon cells although to a lesser degree. Short-axon cells are also a heterogeneous class of neurons. One subgroup of short-axon cells forms inhibitory interglomerular connections (Kiyokage *et al.* 2010, Whitesell *et al.* 2013, Nagayama *et al.* 2014, figure 6). In this subgroup AMPA receptor-mediated currents are likely reduced by CKAMP44 deletion, since these cells show a high TH expression and TH positive cells showed high CKAMP44 mRNA levels. Reduced activity of this subgroup would decrease inhibition of external tufted cells and thereby increase the activity of mitral cells in other glomeruli (Whitesell *et al.* 2013, Kiyokage *et al.* 2010). The hypothesized function of this interglomerular inhibition is to normalize mitral cell activity to overall glomerular activation. This normalization is important to keep mitral cell ensembles comparably stable across different odor concentrations (Linster *&* Cleland 2009). CKAMP44 deletion might interfere with this normalization and reduce independence of mitral cell ensembles from odor concentration. The model used in this study did not include short-axon cells. A more complex model could be used to predict the effect of CKAMP44 deletion on mitral cell activity. The influence of the changed short-axon cell excitability on the experiments performed in this study should be much lower than the impact of the changes in periglomerular cells, since AMPA receptor function was less strongly affected in superficial short-axon cells than in periglomerular cells. Furthermore, in

electrophysiological recordings stimulations were employed to activate mainly one glomerulus. The influence of short-axon cells on odor discrimination should also be less than that of periglomerular cells, considering that the primary function of periglomerular cells is hypothesized to be contrast enhancement (Linster & Cleland 2009).

In addition to the direct effect of CKAMP44 deletion on interglomerular signaling, granule cell activity is indirectly affected. Computational modeling showed that the increased mitral cell activity results in an increased granule cell activity (figure 22). Thereby, granule cell feedback inhibition onto mitral cells is increased and partly compensates for the decreased inhibition by periglomerular cells. Importantly, granule cells not only inhibit cells of one glomerulus, but also mitral cells of other glomeruli (Yokoi *et al.* 1995). These connections are hypothesized to be relevant for contrast enhancement (Mori *et al.* 1999). Therefore, enhanced granule cell activity might also compensate for the decreased non-topographical contrast enhancement due to CKAMP44 deletion. In line with this possible explanation, Nunes & Kuner (2015) showed that increased granule cell activity decreases odor discrimination time.

It is surprising that changes in granule cell but not periglomerular cell activity influence odor discrimination time considering that computational modeling by Gilra & Bhalla predicted that periglomerular cells have a much more pronounced effect on mitral cell activity than granule cells. Periglomerular cells might be relevant at lower odor concentrations, as discussed earlier. Alternatively, increased inhibition of mitral cells as employed by Nunes & Kuner might also be harder to compensate for than reduced inhibition as employed by me.

4.4 Summary

CKAMP44 influences network activity in the olfactory bulb. AMPA receptor mediated-currents in periglomerular cells and to a lesser degree superficial short-axon cells are decreased by CKAMP44 deletion. This decreased excitability of periglomerular cells in turn decreases the inhibition of mitral cells from periglomerular cells. A computation model of the olfactory bulb corroborates these findings. In my thesis, I showed for the first time that the effect of CKAMP44 on AMPA receptor-mediated currents is sufficient to affect the activity of other cells in a neuronal network.

Behavior experiments showed that the function of the olfactory bulb, at least concerning the differentiation of odors at the tested concentrations, is not affected by decreased periglomerular cell excitability. Whether other odor related functions, e.g. detection threshold and odor differentiation at other odor concentrations, are affected remains to be investigated.

Hence, my thesis gained insights into periglomerular cell function in the olfactory bulb network. Periglomerular cells are relevant for controlling mitral cell activity. This is in accordance with previous predictions from modeling (Gilra & Bhalla 2015, Arruda *et al.* 2013). In odor discrimination, a reduced excitability of periglomerular cells seems to play only a minor role or the network is very robustly built and can compensate for reductions in periglomerular cell activity. Periglomerular cells might affect odor discrimination only at low odor concentrations according to the adapted computational model.

List of figures

List of abbreviations

ACSF	artificial cerebrospinal fluid
APV	2-amino-5-phosphonovaleriansäure
AUC	area und the curve
CB	calbindin
CKAMPs	*cystine-knot* AMPA receptor-modulating proteins
CNIH	cornichon homolog
CR	calretinin
DEPC	diethyl pyrocarbonate
EPSC	excitatory postsynaptic current
FISH	fluorescent *in situ* hybridization
GAD67	glutamate dehydrogenase 67
GSG1L	germ cell-specific gene 1-like protein
IPSC	inhibitory postsynaptic current
IR	infra-red
ITI	inter-trial interval
LGN	lateral geniculate nucleus
mEPSC	miniature excitatory postsynaptic currents
PBS	phosphate-buffered saline
PSP	postsynaptic potential
RT	room temperature
TARPs	transmembrane *AMPA* receptor regulatory proteins
TH	tyrosine hydroxylase
TTX	tetrodotoxin

References

Abraham, N. M., Spors, H., Carleton, A., Margrie, T. W., Kuner, T., & Schaefer, A. T. (2004). Maintaining accuracy at the expense of speed: Stimulus similarity defines odor discrimination time in mice. *Neuron*, *44*(5), 865–876. https://doi.org/10.1016/j.neuron.2004.11.017

Allen, K., & Monyer, H. (2015). Interneuron control of hippocampal oscillations. In *Current Opinion in Neurobiology* (Vol. 31, pp. 81–87). Elsevier Ltd. https://doi.org/10.1016/j.conb.2014.08.016

Arruda, D., Publio, R., & Roque, A. C. (2013). The Periglomerular Cell of the Olfactory Bulb and its Role in Controlling Mitral Cell Spiking: A Computational Model. *PLoS ONE*, *8*(2). https://doi.org/10.1371/journal.pone.0056148

Boudkkazi, S., Brechet, A., Schwenk, J., & Fakler, B. (2014). Cornichon2 Dictates the Time Course of Excitatory Transmission at Individual Hippocampal Synapses. *Neuron*, *82*(4), 848–858. https://doi.org/10.1016/j.neuron.2014.03.031

Chen, W. R., Shen, G. Y., Shepherd, G. M., Hines, M. L., & Midtgaard, J. (2002). Multiple modes of action potential initiation and propagation in mitral cell primary dendrite. *Journal of Neurophysiology*, *88*(5), 2755–2764. https://doi.org/10.1152/jn.00057.2002

Chen, X., Aslam, M., Gollisch, T., Allen, K., & Von Engelhardt, J. (2018). CKAMP44 modulates integration of visual inputs in the lateral geniculate nucleus. *Nature Communications*, *9*(1), 1–13. https://doi.org/10.1038/s41467-017-02415-1

Christie, J. M., Bark, C., Hormuzdi, S. G., Helbig, I., Monyer, H., & Westbrook, G. L. (2005). Connexin36 mediates spike synchrony in olfactory bulb glomeruli. *Neuron*, *46*(5), 761–772. https://doi.org/10.1016/j.neuron.2005.04.030

Cleland, T. A., & Linster, C. (2005). Computation in the olfactory system. *Chemical Senses*, *30*(9), 801–813. https://doi.org/10.1093/chemse/bji072

Cleland, T. A., & Sethupathy, P. (2006). Non-topographical contrast enhancement in the olfactory bulb. *BMC Neuroscience*, *7*. https://doi.org/10.1186/1471-2202-7-7

De Saint Jan, D., Hirnet, D., Westbrook, G. L., & Charpak, S. (2009). External tufted cells drive the output of olfactory bulb glomeruli. *Journal of Neuroscience*, *29*(7), 2043–2052. https://doi.org/10.1523/JNEUROSCI.5317-08.2009

Engelhardt, J. Von. (2019). AMPA Receptor Auxiliary Proteins of the CKAMP Family. *International Journal of Molecular Sciences*. https://doi.org/10.3390/ijms20061460

Farrow, P., Khodosevich, K., Sapir, Y., Schulmann, A., Aslam, M., & Stern-bach, Y. (2015). Auxiliary subunits of the CKAMP family differentially modulate AMPA receptor properties. *ELife*, 1–16.

Gaillard, I., Rouquier, S., & Giorgi, D. (2004). Olfactory receptors. In *Cellular and Molecular Life Sciences* (Vol. 61, Issue 4, pp. 456–469). Cell Mol Life Sci. https://doi.org/10.1007/s00018-003-3273-7

Gilra, A., & Bhalla, U. S. (2015). Bulbar microcircuit model predicts connectivity and roles of interneurons in odor coding. *PLoS ONE*, *10*(5), 1–40. https://doi.org/10.1371/journal.pone.0098045

Granseth, B., Ahlstrand, E., & Lindström, S. (2002). Paired pulse facilitation of corticogeniculate EPSCs in the dorsal lateral geniculate nucleus of the rat investigated in vitro. *Journal of Physiology*, *544*(2), 477–486. https://doi.org/10.1113/jphysiol.2002.024703

Hayar, A., Karnup, S., Ennis, M., & Shipley, M. T. (2004). External tufted cells: A major excitatory element that coordinates glomerular activity. *Journal of Neuroscience*, *24*(30), 6676–6685. https://doi.org/10.1523/JNEUROSCI.1367-04.2004

Heyward, P., Ennis, M., Keller, A., & Shipley, M. T. (2001). Membrane bistability in olfactory bulb mitral cells. *Journal of Neuroscience*, *21*(14), 5311–5320. https://doi.org/10.1523/jneurosci.21-14-05311.2001

Imai, T., Sakano, H., & Vosshall, L. B. (2010). Topographic Mapping — The Olfactory System. *Cold Spring Harbor Perspectives in Biology*, 1–18.

Jackson, A. C., & Nicoll, R. A. (2011). The Expanding Social Network of Ionotropic Glutamate Receptors: TARPs and Other Transmembrane Auxiliary Subunits. In *Neuron* (Vol. 70, Issue 2, pp. 178–199). Neuron. https://doi.org/10.1016/j.neuron.2011.04.007

Jacobi, E., & von Engelhardt, J. (2017). Diversity in AMPAR complexes in the brain. *Current Opinion in Neurobiology*, *45*, 32–38. https://doi.org/10.1016/j.conb.2017.03.001

Källman, A. M., Sahlin, M., & Öhman, M. (2003). ADAR2 A→I editing: Site selectivity and editing efficiency are separate events. *Nucleic Acids Research*, *31*(16), 4874–4881. https://doi.org/10.1093/nar/gkg681

Kato, A. S., Gill, M. B., Ho, M. T., Yu, H., Tu, Y., Siuda, E. R., Wang, H., Qian, Y. W., Nisenbaum, E. S., Tomita, S., & Bredt, D. S. (2010). Hippocampal AMPA Receptor Gating Controlled by Both TARP and Cornichon Proteins. *Neuron*, *68*(6), 1082–1096. https://doi.org/10.1016/j.neuron.2010.11.026

Kee, T., Sanda, P., Gupta, N., Stopfer, M., & Bazhenov, M. (2015). Feed-Forward versus Feedback Inhibition in a Basic Olfactory Circuit. *PLoS Computational Biology*, *11*(10), 1–24. https://doi.org/10.1371/journal.pcbi.1004531

Kessels, H. W., Kopec, C. D., Klein, M. E., & Malinow, R. (2009). Roles of stargazin and phosphorylation in the control of AMPA receptor subcellular distribution. *Nature Neuroscience*, *12*(7), 888–896. https://doi.org/10.1038/nn.2340

Khodosevich, K., Jacobi, E., Farrow, P., Schulmann, A., Rusu, A., Zhang, L., Sprengel, R., Monyer, H., & von Engelhardt, J. (2014). Coexpressed Auxiliary Subunits Exhibit Distinct

Modulatory Profiles on AMPA Receptor Function. *Neuron*, *83*(3), 601–615. https://doi.org/10.1016/j.neuron.2014.07.004

Kiyokage, E., Pan, Y. Z., Shao, Z., Kobayashi, K., Szabo, G., Yanagawa, Y., Obata, K., Okano, H., Toida, K., Puche, A. C., & Shipley, M. T. (2010). Molecular identity of periglomerular and short axon cells. *Journal of Neuroscience*, *30*(3), 1185–1196. https://doi.org/10.1523/JNEUROSCI.3497-09.2010

Koike-Tani, M., Kanda, T., Saitoh, N., Yamashita, T., & Takahashi, T. (2008). Involvement of AMPA receptor desensitization in short-term synaptic depression at the calyx of Held in developing rats. *Journal of Physiology*, *586*(9), 2263–2275. https://doi.org/10.1113/jphysiol.2007.142547

Kosaka, K., Toida, K., Margolis, F. L., & Kosaka, T. (1996). Chemically defined neuron groups and their subpopulations in the glomerular layer of the rat main olfactory bulb - II. Prominent differences in the intraglomerular dendritic arborization and their relationship to olfactory nerve terminals. *Neuroscience*, *76*(3), 775–786. https://doi.org/10.1016/S0306-4522(96)00308-9

Kosaka, K., & Kosaka, T. (2007). Chemical properties of type 1 and type 2 periglomerular cells in the mouse olfactory bulb are different from those in the rat olfactory bulb. *Brain Research*, *1167*(1), 42–55. https://doi.org/10.1016/j.brainres.2007.04.087

Kosaka, K., & Kosaka, T. (2004). Organization of the Main Olfactory Bulbs of Some Mammals: Musk Shrews, Moles, Hedgehogs, Tree Shrews, Bats, Mice, and Rats. *Journal of Comparative Neurology*, *472*(1), 1–12. https://doi.org/10.1002/cne.20004

Kosaka, K., Toida, K., Aika, Y., & Kosaka, T. (1998). How simple is the organization of the olfactory glomerulus?: The heterogeneity of so-called periglomerular cells. *Neuroscience Research*, *30*(2), 101–110. https://doi.org/10.1016/S0168-0102(98)00002-9

Lein, E. S., Hawrylycz, M. J., Ao, N., Ayres, M., Bensinger, A., Bernard, A., Boe, A. F., Boguski, M. S., Brockway, K. S., Byrnes, E. J., Chen, L., Chen, L., Chen, T. M., Chin, M. C., Chong, J., Crook, B. E., Czaplinska, A., Dang, C. N., Datta, S., … Jones, A. R. (2007). Genome-wide atlas of gene expression in the adult mouse brain. *Nature*, *445*(7124), 168–176. https://doi.org/10.1038/nature05453

Li, G., & Cleland, T. A. (2017). A coupled-oscillator model of olfactory bulb gamma oscillations. In *PLoS computational biology* (Vol. 13, Issue 11). https://doi.org/10.1371/journal.pcbi.1005760

Linster, C., & Cleland, T. A. (2009). Glomerular microcircuits in the olfactory bulb. *Neural Networks*, *22*(8), 1169–1173. https://doi.org/10.1016/j.neunet.2009.07.013

Lledo, P. M., Alonso, M., & Grubb, M. S. (2006). Adult neurogenesis and functional plasticity in neuronal circuits. *Nature Reviews Neuroscience*, *7*(3), 179–193. https://doi.org/10.1038/nrn1867

Mazor, O., & Laurent, G. (2005). Transient dynamics versus fixed points in odor representations by locust antennal lobe projection neurons. *Neuron*, *48*(4), 661–673. https://doi.org/10.1016/j.neuron.2005.09.032

Menini, A., Lagostena, L., & Boccaccio, A. (2004). Olfaction: From odorant molecules to the olfactory cortex. *News in Physiological Sciences*, *19*(3), 101–104. https://doi.org/10.1152/nips.1507.2003

Montague, A. A., & Greer, C. A. (1999). Differential distribution of ionotropic glutamate receptor subunits in the rat olfactory bulb. *Journal of Comparative Neurology*, *405*(2), 233–246. https://doi.org/10.1002/(SICI)1096-9861(19990308)405:2<233::AID-CNE7>3.0.CO;2-A

Monyer, H., Seeburg, P. H., & Wisden, W. (1991). Glutamate-operated channels: Developmentally early and mature forms arise by alternative splicing. *Neuron*, *6*(5), 799–810. https://doi.org/10.1016/0896-6273(91)90176-Z

Mori, K., Kishi, K., & Ojima, H. (1983). Distribution of dendrites of mitral, displaced mitral, tufted, and granule cells in the rabbit olfactory bulb. *Journal of Comparative Neurology*, *219*(3), 339–355. https://doi.org/10.1002/cne.902190308

Mori, K., Nagao, H., & Yoshihara, Y. (1999). The olfactory bulb: Coding and processing of odor molecule information. In *Science* (Vol. 286, Issue 5440, pp. 711–715). American Association for the Advancement of Science. https://doi.org/10.1126/science.286.5440.711

Mori, K., Takahashi, Y. K., Igarashi, K. M., & Yamaguchi, M. (2006). Maps of odorant molecular features in the mammalian olfactory bulb. *Physiological Reviews*, *86*(2), 409–433. https://doi.org/10.1152/physrev.00021.2005

Murphy, G. J., Darcy, D. P., & Isaacson, J. S. (2005). Intraglomerular inhibition: Signaling mechanisms of an olfactory microcircuit. *Nature Neuroscience*, *8*(3), 354–364. https://doi.org/10.1038/nn1403

Murphy, G. J., Glickfeld, L. L., Balsen, Z., & Isaacson, J. S. (2004). Sensory Neuron Signaling to the Brain: Properties of Transmitter Release from Olfactory Nerve Terminals. *Journal of Neuroscience*, *24*(12), 3023–3030. https://doi.org/10.1523/JNEUROSCI.5745-03.2004

Nagayama, S., Homma, R., & Imamura, F. (2014). Neuronal organization of olfactory bulb circuits. *Frontiers in Neural Circuits*, *8*(SEP), 1–19. https://doi.org/10.3389/fncir.2014.00098

Niimura, Y., & Nei, M. (2007). Extensive gains and losses of olfactory receptor genes in mammalian evolution. *PLoS ONE*, *2*(8). https://doi.org/10.1371/journal.pone.0000708

Nunes, D., & Kuner, T. (2015). Disinhibition of olfactory bulb granule cells accelerates odour discrimination in mice. *Nature Communications*, *6*. https://doi.org/10.1038/ncomms9950

Pachernegg, S., Münster, Y., Muth-Köhne, E., Fuhrmann, G., & Hollmann, M. (2015). GluA2 is rapidly edited at the Q/R site during neural differentiation in vitro. *Frontiers in Cellular Neuroscience*, *9*(March), 1–14. https://doi.org/10.3389/fncel.2015.00069

Parrish-Aungst, S., Shipley, M. T., Erdelyi, F., Szabo, G., & Puche, A. C. (2007). Quantitative analysis of neuronal diversity in the mouse olfactory bulb. *Journal of Comparative Neurology*, *501*(6), 825–836. https://doi.org/10.1002/cne.21205

Pinching, A. J., & Powell, T. P. (1971). The neuron types of the glomerular layer of the olfactory bulb. *Journal of Cell Science*, *9*(2), 305–345.

Price, J. L., & Powell, T. P. (1970). The mitral and short axon cells of the olfactory bulb. *Journal of Cell Science*, *7*(3), 631–651.

Regehr, W. G. (2012). Short-term presynaptic plasticity. *Cold Spring Harbor Perspectives in Biology*, *4*(7), 1–19. https://doi.org/10.1101/cshperspect.a005702

Reinert, J. K., Schaefer, A. T., & Kuner, T. (2019). High-Throughput Automated Olfactory Phenotyping of Group-Housed Mice. *Frontiers in Behavioral Neuroscience*, *13*(December), 1–13. https://doi.org/10.3389/fnbeh.2019.00267

Rosenmund, C., Stern-Bach, Y., & Stevens, C. F. (1998). The tetrameric structure of a glutamate receptor channel. *Science*, *280*(5369), 1596–1599. https://doi.org/10.1126/science.280.5369.1596

Schoppa, N. E., & Westbrook, G. L. (2001). Glomerulus-specific synchronization of mitral cells in the olfactory bulb. *Neuron*, *31*(4), 639–651. https://doi.org/10.1016/S0896-6273(01)00389-0

Schwenk, J., Harmel, N., Brechet, A., Zolles, G., Berkefeld, H., Müller, C. S., Bildl, W., Baehrens, D., Hüber, B., Kulik, A., Klöcker, N., Schulte, U., & Fakler, B. (2012). High-Resolution Proteomics Unravel Architecture and Molecular Diversity of Native AMPA Receptor Complexes. *Neuron*, *74*(4), 621–633. https://doi.org/10.1016/j.neuron.2012.03.034

Schwenk, J., Harmel, N., Zolles, G., Bildl, W., Kulik, A., Heimrich, B., Chisaka, O., Jonas, P., Schulte, U., Fakler, B., & Klöcker, N. (2009). Functional proteomics identify cornichon proteins as auxiliary subunits of AMPA receptors. *Science*, *323*(5919), 1313–1319. https://doi.org/10.1126/science.1167852

Scott, J. W., Wellis, D. P., Riggott, M. J., & Buonviso, N. (1993). Functional organization of the main olfactory bulb. *Microscopy Research and Technique*, *24*(2), 142–156. https://doi.org/10.1002/jemt.1070240206

Shao, Z., Puche, A. C., Kiyokage, E., Szabo, G., & Shipley, M. T. (2009). Two GABAergic intraglomerular circuits differentially regulate tonic and phasic presynaptic inhibition of olfactory nerve terminals. *Journal of Neurophysiology*, *101*(4), 1988–2001. https://doi.org/10.1152/jn.91116.2008

Shen, G. Y., Chen, W. R., Midtgaard, J., Shepherd, G. M., & Hines, M. L. (1999). Computational analysis of action potential initiation in mitral cell soma and dendrites based on dual patch recordings. *Journal of Neurophysiology*, *82*(6), 3006–3020. https://doi.org/10.1152/jn.1999.82.6.3006

Sommer, B., Keinänen, K., Verdoorn, T. A., Wisden, W., Burnashev, N., Herb, A., Köhler, M., Takagi, T., Sakmann, B., & Seeburg, P. H. (1990). Flip and flop: A cell-specific functional switch in glutamate-operated channels of the CNS. *Science*, *249*(4976), 1580–1585. https://doi.org/10.1126/science.1699275

Sorge, R. E., Martin, L. J., Isbester, K. A., Sotocinal, S. G., Rosen, S., Tuttle, A. H., Wieskopf, J. S., Acland, E. L., Dokova, A., Kadoura, B., Leger, P., Mapplebeck, J. C. S., McPhail, M., Delaney, A., Wigerblad, G., Schumann, A. P., Quinn, T., Frasnelli, J., Svensson, C. I., … Mogil, J. S. (2014). Olfactory exposure to males, including men, causes stress and related analgesia in rodents. *Nature Methods*, *11*(6), 629–632. https://doi.org/10.1038/nmeth.2935

Stell, B. M., & Mody, I. (2002). Receptors with different affinities mediate phasic and tonic GABA(A) conductances in hippocampal neurons. *The Journal of Neuroscience : The Official Journal of the Society for Neuroscience*, *22*(10), 1–5. https://doi.org/10.1523/jneurosci.22-10-j0003.2002

Swanson, G. T., Kamboj, S. K., & Cull-Candy, S. G. (1997). Single-channel properties of recombinant AMPA receptors depend on RNA editing, splice variation, and subunit composition. *Journal of Neuroscience*, *17*(1), 58–69. https://doi.org/10.1523/jneurosci.17-01-00058.1997

Tomita, S., Chen, L., Kawasaki, Y., Petralia, R. S., Wenthold, R. J., Nicoll, R. A., & Bredt, D. S. (2003). Functional studies and distribution define a family of transmembrane AMPA receptor regulatory proteins. *Journal of Cell Biology*, *161*(4), 805–816. https://doi.org/10.1083/jcb.200212116

Treloar, H. B., Feinstein, P., Mombaerts, P., & Greer, C. A. (2002). Specificity of Glomerular Targeting by Olfactory Sensory Axons. *Journal of Neuroscience*, *22*(7), 2469–2477. https://doi.org/10.1523/jneurosci.22-07-02469.2002

Urban, N. N., & Sakmann, B. (2002). Reciprocal intraglomerular excitation and intra- and interglomerular lateral inhibition between mouse olfactory bulb mitral cells. *Journal of Physiology*, *542*(2), 355–367. https://doi.org/10.1113/jphysiol.2001.013491

Von Engelhardt, J., Mack, V., Sprengel, R., Kavenstock, N., Li, K. W., Stern-Bach, Y., Smit, A. B., Seeburg, P. H., & Monyer, H. (2010). CKAMP44: A brain-specific protein attenuating short-term synaptic plasticity in the dentate gyrus. *Science*, *327*(5972), 1518–1522. https://doi.org/10.1126/science.1184178

Wang, J. Q., Arora, A., Yang, L., Parelkar, N. K., Zhang, G., Liu, X., Eun, S. C., & Mao, L. (2005). Phosphorylation of AMPA receptors: Mechanisms and synaptic plasticity. *Molecular Neurobiology*, *32*(3), 237–249. https://doi.org/10.1385/MN:32:3:237

Weiss, T., Soroka, T., Gorodisky, L., Shushan, S., Snitz, K., Weissgross, R., Furman-Haran, E., Dhollander, T., & Sobel, N. (2020). Human Olfaction without Apparent Olfactory Bulbs. *Neuron*, *105*(1), 35-45.e5. https://doi.org/10.1016/j.neuron.2019.10.006

Whitesell, J. D., Sorensen, K. A., Jarvie, B. C., Hentges, S. T., & Schoppa, N. E. (2013). Interglomerular lateral inhibition targeted on external tufted cells in the olfactory bulb. *Journal of Neuroscience*, *33*(4), 1552–1563. https://doi.org/10.1523/JNEUROSCI.3410-12.2013

Wicher, D. (2012). Functional and evolutionary aspects of chemoreceptors. *Frontiers in Cellular Neuroscience*, *6*(OCTOBER 2012), 1–13. https://doi.org/10.3389/fncel.2012.00048

Wright, A., & Vissel, B. (2012). The essential role of AMPA receptor GluA2 subunit RNA editing in the normal and diseased brain. *Frontiers in Molecular Neuroscience*, *5*(APRIL), 1–13. https://doi.org/10.3389/fnmol.2012.00034

Yamada, K. A., & Tang, C. M. (1993). Benzothiadiazides inhibit rapid glutamate receptor desensitization and enhance glutamatergic synaptic currents. *Journal of Neuroscience*, *13*(9), 3904–3915. https://doi.org/10.1523/jneurosci.13-09-03904.1993

Yokoi, M., Mori, K., & Nakanishi, S. (1995). Refinement of odor molecule tuning by dendrodendritic synaptic inhibition in the olfactory bulb. *Proceedings of the National Academy of Sciences of the United States of America*, *92*(8), 3371–3375. https://doi.org/10.1073/pnas.92.8.3371